StaR and FLAiR: Stabilizing and Enriching Randomized Neural Networks

Anonymous authors
Paper under double-blind review

Abstract

Randomized neural networks (RdNNs) surpass conventional deep models in efficiency by freezing randomly initialized input-to-hidden weights, which permits a closed-form output-layer solution and eliminates the need for backpropagation. However, they often suffer from instability and limited representation quality due to unregulated weight initialization and fixed, non-adaptive hidden mappings. Despite their widespread use, the lack of principled mechanisms to stabilize random mappings and enrich hidden representations remains largely unaddressed. To tackle these foundational issues, we introduce two novel, theoretically grounded frameworks, marking the first attempt to stabilize and enrich RdNN representations. First, **`StaR`** (**`Sta`**ble **`R`**epresentations) mechanism that regulates the spectrum of input-to-hidden random weight matrix by constraining singular values to a bounded interval, yielding well-conditioned hidden mappings that curb noise amplification and feature suppression. Second, **`FLAiR`** (**`F`**ew-step **`L`**earning for **`A`**daptive **`I`**nitialization and **`R`**epresentation) mechanism that applies a small, fixed number of gradient steps to input-to-hidden weights before freezing them, lightly adapting nonlinear features to task structure without incurring full backpropagation costs. We evaluate both frameworks on 146 diverse benchmark datasets, covering both binary and multiclass classification tasks using standard shallow and deep RdNN architectures. Extensive empirical results demonstrate that our methods significantly improve accuracy, stability, and generalization, while preserving the efficiency of RdNNs. Furthermore, we provide theoretical guarantees showing that **`StaR`** yields bounded spectral norms and well-conditioned hidden-layer transformations, and that **`FLAiR`** enhances representation quality through limited adaptation. Codes for baseline and **`StaR`**/**`FLAiR`**-enhanced models are provided in the supplementary file.

1 Introduction

The remarkable success of deep learning (DL) models in diverse domains, ranging from image recognition Voulodimos et al. (2018); Chen et al. (2019); Liu et al. (2024) to natural language processing Otter et al. (2021); Lauriola et al. (2022); Yin et al. (2024) stems from their ability to learn complex patterns and representations through hierarchical feature extraction LeCun et al. (2015); Luo et al. (2023). By minimizing task-specific loss functions via backpropagation and gradient-based optimization, these networks iteratively refine their parameters to learn hierarchical and expressive representations of the data. However, achieving state-of-the-art performance with deep models often requires substantial computational resources, extensive hyperparameter tuning, and long training times Goodfellow et al. (2016); Tiwari et al. (2023). Furthermore, training deep architectures can be hindered by the vanishing or exploding gradient problem Pascanu et al. (2013); Jaiswal et al. (2022); Ceni (2025).

The aforementioned limitations of DL models have prompted researchers to seek alternative neural architectures that combine predictive performance with greater computational efficiency. One promising family of approaches is randomized neural networks (RdNNs) Pao et al. (1994); Cao et al. (2018); Suganthan & Katuwal (2021); Hu et al. (2024). In contrast to conventional deep models trained by backpropagation, RdNNs randomly initialize a substantial subset of their parameters (typically the hidden-layer weights), which are then held fixed, while the remaining (often output) parameters are computed analytically in closed form. This paradigm eliminates the need for iterative weight updates, substantially reducing training time and computational overhead, yet still allows RdNNs to learn complex input-output mappings Zhang & Suganthan (2016). Notably, despite their simplicity, RdNNs retain the universal approximation property, enabling them to approximate any continuous function on a compact domain arbitrarily well given sufficient hidden nodes and suitable activations Igelnik & Pao (1995); Needell et al. (2024).

In recent years, RdNNs have witnessed significant advancements, particularly in methods aimed at improving their robustness and scalability. Ensemble-based approaches have been introduced to enhance generalization and mitigate the variability Shi et al. (2021), Guo et al. (2021). Granular ball-based scalable methods have further extended the applicability of RdNNs to large-scale and high-dimensional datasets Sajid et al. (2025a). Additionally, the integration of fuzzy inference systems into RdNN frameworks has provided a way to incorporate uncertainty handling and interpretability, making them more effective for complex and imprecise decision-making tasks Sajid et al. (2024b; 2025b).

Despite several advancements, RdNNs continue to face fundamental issues stemming from fixed, randomly initialized input-to-hidden weights, which can produce poorly conditioned hidden representations, amplify input noise, and result in instability and inconsistent performance across datasets Li & Wang (2017); Scardapane & Wang (2017). Yet, no principled framework has been proposed to regulate the randomness at the heart of RdNNs. The core challenges arising from unregulated and fixed randomness—namely, ill-conditioned hidden representations and high variability in learned features—are formally articulated in Problem Statements **`P1`** and **`P2`**, which are elaborated in the subsequent section.

Although techniques such as better initialization Glorot & Bengio (2010), orthogonalization Saxe et al. (2013), and spectral normalization Miyato et al. (2018) have been proposed to mitigate instability in traditional deep networks—where weights are iteratively updated via backpropagation—these methods are tailored for gradient-based optimization and are not applicable to RdNNs, where weights remain fixed after random initialization. Within the RdNN paradigm, limited efforts have been made to address the instability and low representational quality that arise from unregulated fixed weights. Regularization techniques, such as ℓ_1 penalties Zhang et al. (2019), and ensemble-based methods Cao et al. (2012), have been explored to improve generalization. However, these approaches primarily operate at the output level, leaving the root causes—namely, unstable hidden transformations and uninformative or poorly expressive hidden representations—unaddressed. To date, no systematic framework has been developed to tackle these limitations directly, leaving a critical gap in the literature.

2 CONTRIBUTIONS

To directly address the core challenges of instability and poor representation quality in RdNNs, we propose two novel frameworks: **`StaR`** (**`Sta`**ble **R**epresentations) and **`FLAiR`** (**`F`**ew-step **`L`**earning for **`A`**daptive **`I`**nitialization and **`R`**epresentation). These frameworks provide the first principled mechanisms to ensure numerical stability and improve representational quality in RdNNs by addressing the effects of fixed randomness.

The **`StaR`** framework is theoretically motivated by insights from *Random Matrix Theory* (RMT) Edelman & Rao (2005); Tao (2012), which provides a rigorous mathematical foundation for characterizing the spectral properties of large random matrices—particularly their singular value distributions. RMT has shown that unstructured random matrices, such as those used in RdNNs, often exhibit extreme singular values, leading to ill-conditioned transformations that amplify noise or suppress informative signals. Drawing on this perspective, **`StaR`** seeks to regulate the spectrum of random input-to-hidden weight matrices, ensuring that the resulting representations are stable and well-conditioned. This spectral regularization strategy directly addresses the core instability and numerical conditioning issues, while preserving the computational simplicity of RdNNs.

The **`FLAiR`** framework is inspired by recent theoretical insights into representation learning in high-dimensional settings. Specifically, the work of Ba et al. Ba et al. (2022) reveals that even a single gradient step can lead to a considerable advantage over random features. While this phenomenon has been studied in iterative training regimes, its implications are particularly valuable for RdNNs, where the input-to-hidden weights are fixed and untrained. **`FLAiR`** harnesses this insight by introducing a lightweight warm-up phase, wherein a small number of gradient steps are applied to the input-to-hidden weights before freezing. This early-stage adaptation promotes task-aware feature extraction and improves the representational capacity of RdNNs without compromising their hallmark efficiency. By doing so, **`FLAiR`** enables RdNNs to move beyond purely random transformations, offering a principled means to inject data-dependent structure into otherwise fixed feature maps.

Together, **`StaR`** and **`FLAiR`** mark the first effort to systematically enhance both the stability and expressiveness of RdNNs—directly at their structural core. By regulating spectral properties and introducing lightweight data-driven adaptation, these methods retain the efficiency of RdNNs while systematically resolving long-standing structural limitations. Notably, both frameworks are architecture-agnostic and can be integrated into any RdNN variant, paving the way for more stable, expressive, and theoretically grounded randomized models.

3 PRELIMINARIES AND PROBLEM DEFINITION

RdNN setting. Let $X \in \mathbb{R}^{m\times d}$ denote the input data matrix with m samples and d features, and let $Y \in \mathbb{R}^{m\times n}$ be the target matrix (e.g., one-hot encoded labels for classification). A RdNN samples a hidden-layer weight matrix $W \in \mathbb{R}^{d\times h}$ from a fixed distribution (typically $\mathcal{U}[-1,1]$ or $\mathcal{N}(0,1)$) and freezes it throughout training. The hidden-layer output is given by

$$H = \phi(XW + B) \in \mathbb{R}^{m\times h}, \tag{1}$$

where $\phi : \mathbb{R} \to \mathbb{R}$ is a nonlinear activation function applied elementwise, and $B \in \mathbb{R}^{m\times h}$ is a bias matrix. The output weights $\Theta \in \mathbb{R}^{h\times n}$ are computed in closed form via regularized least squares:

$$\begin{aligned}\Theta^\star(W) &= \arg\min_{\Theta} \ \|H\Theta - Y\|_F^2 + \lambda\|\Theta\|_F^2 \\ &= (H^\top H + \lambda I_h)^{-1} H^\top Y, \end{aligned} \tag{2}$$

where $\lambda \geq 0$ is a regularization parameter. The above formulation captures the core learning structure shared by a wide class of RdNN models, where training reduces to solving a linear system after a fixed random feature transformation. Detailed formulation and architecture of standard RdNN models are discussed in Section A of the Appendix.

Spectral preliminaries. The stability and expressiveness of RdNNs critically depend on the spectral properties of the random weight matrix W. Let $W = U \cdot \Sigma \cdot V^\top$ be the singular value decomposition (SVD) of W, where $\Sigma = \mathrm{diag}(\sigma_1, \ldots, \sigma_r)$ contains the singular values of W, and $r = \min(d, h)$. The spectral norm $\|W\|_2 = \sigma_{\max}$ determines the maximum amplification of input directions, while the smallest singular value $\sigma_{\min}$ controls the degree of contraction. The condition number $\kappa(W) = \sigma_{\max}/\sigma_{\min}$ quantifies the sensitivity of matrix inversion to perturbations and is a standard measure of numerical stability Golub & Van Loan (2013). An ill-conditioned W, characterized by a large condition number, can lead to unstable or poorly scaled hidden-layer representations H Zhang et al. (2018). These problems amplify noise, suppress informative features, and degrade the numerical stability of the closed-form solution in equation 2. Moreover, excessive variation in spectral norms across initializations contributes to inconsistent performance.

PROBLEM STATEMENT

`P1`: Spectral Instability and Poor Conditioning. In RdNNs, the hidden-layer transformation $H = \phi(XW + B)$ is governed by the spectral structure of the randomly initialized matrix W. Unregulated W may exhibit heavy-tailed or degenerate singular spectra, causing (i) noise amplification (large $\sigma_{\max}$), (ii) feature suppression (small $\sigma_{\min}$), and (iii) numerical instability in solving equation 2 (large $\kappa(W)$). These issues can severely degrade the stability and robustness of RdNNs. The core objective is thus to *stabilize* the hidden-layer transformation by enforcing a controlled and well-conditioned singular spectrum in W.

`P2`: Inflexible Representations from Frozen Random Weights. While fixing the random weight matrix W allows RdNNs to avoid iterative backpropagation and enjoy efficient closed-form training, it inherently limits the expressiveness and task-specific alignment of the hidden transformation

$H = \phi(XW + B)$. Since W is sampled randomly and remains frozen, the resulting feature representations may fail to learn discriminative patterns essential for the downstream task. Additionally, the randomness of W induces high variability in performance across different initializations, compromising model reliability. The fundamental challenge is thus to enrich the representational quality of H by enabling limited, computationally light adaptation of W, without sacrificing the efficiency of closed-form training.

4 METHOD

To address the limitations identified in `P1` (spectral instability) and `P2` (inflexible representations), we propose two frameworks:

- **`StaR`** (***Sta**ble **R**epresentations*) directly targets `P1` by enforcing spectral regularity in the random weight matrix W. It projects the singular values of W onto a prescribed bounded interval, yielding a well-conditioned transformation H that mitigates both noise amplification and feature suppression.
- **`FLAiR`** (***F**ew-step **L**earning for **A**daptive **I**nitialization and **R**epresentation*) addresses `P2` by introducing a lightweight adaptation stage. A small number of gradient updates refine W before freezing, enabling task-aware hidden-layer representations without sacrificing closed-form output-layer training.

While **`StaR`** and **`FLAiR`** are designed to address `P1` and `P2` respectively, both frameworks contribute to improving the hidden transformation $H = \phi(XW + B)$ through distinct mechanisms. We now describe each framework in detail.

4.1 **STAR**: **STA**BLE **R**EPRESENTATIONS

`StaR` is a principled singular value regulation mechanism designed to mitigate spectral pathologies in RdNNs by projecting the spectrum of the randomly initialized weight matrix $W \in \mathbb{R}^{d \times h}$ onto a bounded interval. This ensures that the resulting hidden-layer transformation $H = \phi(XW + B)$ remains well-conditioned, thereby addressing `P1`. The detailed steps of the **`StaR`** framework are as follows:

1. **Singular value decomposition:** The randomly initialized weight matrix $W \in \mathbb{R}^{d \times h}$ is decomposed as:
$$W = U \cdot \Sigma \cdot V^{\top},$$
where $U \in \mathbb{R}^{d \times d}$ and $V \in \mathbb{R}^{h \times h}$ are orthogonal matrices containing the left and right singular vectors of W, and $\Sigma = \text{diag}(\sigma_1, \sigma_2, \ldots, \sigma_r)$ is a diagonal matrix of singular values with $\sigma_i \geq 0$.
2. **Singular value rescaling:** To improve the conditioning of the weight matrix and ensure stable transformations, the singular values in Σ are linearly rescaled to lie within a target interval $[\sigma_{\text{low}},\ \sigma_{\text{high}}]$, where $\sigma_{\text{low}} > 0$. This guarantees that the singular values of the regulated matrix W' satisfy:
$$\sigma_{\text{low}} \leq \sigma'_i \leq \sigma_{\text{high}}, \quad \forall i \in \{1, 2, \ldots, r\}. \tag{3}$$
The rescaled singular values are computed as:
$$\sigma'_i = \frac{\sigma_i - \sigma_{\min}}{\sigma_{\max} - \sigma_{\min} + \varepsilon} \cdot (\sigma_{\text{high}} - \sigma_{\text{low}}) + \sigma_{\text{low}}, \;\; \forall i, \tag{4}$$
where $\sigma_{\min} = \min_i \sigma_i$, $\sigma_{\max} = \max_i \sigma_i$, and ε is a small constant added for numerical stability.

   Conditioning Guarantee: As a result of this bounded rescaling, the condition number of the regulated matrix is explicitly controlled:
$$\kappa(W') = \frac{\sigma_{\text{high}}}{\sigma_{\text{low}}}, \tag{5}$$

Algorithm 1 StaR: Stable Representation via Spectral Rescaling

```
Input: Random weight matrix $W \in \mathbb{R}^{d\times h}$; spectral bounds $\sigma_{\text{low}} > 0$, $\sigma_{\text{high}} > \sigma_{\text{low}}$
Output: Regulated matrix $W' \in \mathbb{R}^{d\times h}$
1. Compute SVD: $W = U \cdot \Sigma \cdot V^\top$
2. Extract singular values: $\Sigma = \text{diag}(\sigma_1, \dots, \sigma_r)$
3. Normalize and Rescale:
    $\sigma_{\min} \leftarrow \min_i \sigma_i, \quad \sigma_{\max} \leftarrow \max_i \sigma_i$
    $\sigma'_i \leftarrow \frac{\sigma_i - \sigma_{\min}}{\sigma_{\max} - \sigma_{\min} + \varepsilon} \cdot (\sigma_{\text{high}} - \sigma_{\text{low}}) + \sigma_{\text{low}}, \quad \forall i$
    $\Sigma' \leftarrow \text{diag}(\sigma'_1, \dots, \sigma'_r)$
4. Reconstruct: $W' = U \cdot \Sigma' \cdot V^\top$
Return: $W'$
```

which prevents ill-conditioning and ensures well-behaved hidden-layer transformations. By avoiding extremely small singular values, **StaR** reduces the risk of feature collapse and information loss, while bounding large singular values mitigates noise amplification and instability.

3. **Reconstruction of the regulated weight matrix:** The regulated weight matrix W' is reconstructed using the rescaled singular values:

$$W' = U \cdot \Sigma' \cdot V^\top, \tag{6}$$

where $\Sigma' = \text{diag}(\sigma'_1, \sigma'_2, \dots, \sigma'_r)$. This procedure preserves the directional geometry encoded by the singular vectors while correcting the pathological scaling in the singular values. The resulting matrix W' ensures stable and well-conditioned hidden transformations, prevents noise amplification and feature suppression.

Algorithm 1 summarizes the **StaR** procedure.

To rigorously characterize the benefits of spectral regulation, we formalize two key advantages of **StaR** in terms of hidden-layer conditioning and stability. Specifically, Lemma 1 (see Appendix B) establishes (i)—that **StaR** controls the condition number of the random weight matrix—while Lemma 2 (see Appendix B) establishes (ii)—that **StaR** induces Lipschitz-continuous transformations, ensuring numerically stable and bounded sensitivity to input perturbations.

These theoretical results formally support the conditioning and stability improvements introduced by **StaR**.

4.2 FLAiR: FEW-STEP LEARNING FOR ADAPTIVE INITIALIZATION AND REPRESENTATION

FLAiR is a general framework for enhancing the representation capacity of RdNN by introducing a short, few-step learning phase for input-to-hidden weights. Instead of relying solely on fixed random projections, **FLAiR** introduces a short warm-up phase wherein the input-to-hidden weights (and biases) are updated using gradient-based optimization for a few epochs. These refined weights are then frozen, and the output weights are subsequently computed in closed-form. This two-stage procedure improves feature alignment, reduces sensitivity to random initialization, and enhances downstream performance, thereby addressing **P2**. The **FLAiR** mechanism comprises the following steps:

1. **Initialization:** Random weights W and biases B are sampled, as per the standard RdNN setup.
2. **Warm-up Training (Few-step Adaptive Update):** To improve representation quality, **FLAiR** introduces a short warm-up phase that adaptively updates the hidden parameters W and B for a small number of steps T using gradient descent (e.g., Adam optimizer). At

Algorithm 2 **`FLAiR`: `F`ew-step `L`earning for `A`daptive `I`nitialization and `R`epresentation**

```
Input: Data matrix $X \in \mathbb{R}^{m \times d}$, target matrix $Y \in \mathbb{R}^{m \times n}$; number of hidden units $h$; activation $\phi(\cdot)$; warm-up epochs $T$; learning rate $\eta$; regularization $\lambda > 0$
Output: Output weights $\Theta \in \mathbb{R}^{h \times n}$; refined weights $W^{(T)}$, $B^{(T)}$
1. Random Initialization: Sample $W^{(0)} \in \mathbb{R}^{d \times h}$, $B^{(0)} \in \mathbb{R}^{1 \times h}$
for $t = 1$ to $T$ do
    a. Hidden Representation: $H^{(t)} = \phi(XW^{(t-1)} + \mathbf{1}B^{(t-1)})$
    b. Closed-form Output Estimation:
        $\Theta^{(t)} = (H^{(t)\top} H^{(t)} + \lambda I_h)^{-1} H^{(t)\top} Y$
    c. Prediction: $\hat{Y}^{(t)} = H^{(t)} \Theta^{(t)}$
    d. Loss Computation: $\mathcal{L}^{(t)} = \|\hat{Y}^{(t)} - Y\|_F^2$
    e. Backpropagation: Update $W^{(t-1)}$, $B^{(t-1)}$ using gradients from $\mathcal{L}^{(t)}$ (e.g., via Adam)
end for
2. Freeze Parameters: $W^{(T)} \leftarrow W^{(T-1)}$, $B^{(T)} \leftarrow B^{(T-1)}$
3. Final Hidden Representation: $H = \phi(XW^{(T)} + \mathbf{1}B^{(T)})$
4. Final Output Learning:
        $\Theta = (H^\top H + \lambda I_h)^{-1} H^\top Y$
Return: $\Theta$, $W^{(T)}$, $B^{(T)}$
```

each warm-up epoch $t = 1, \ldots, T$, the current hidden features are computed as:

$$H^{(t)} = \phi(XW^{(t)} + B^{(t)}) \in \mathbb{R}^{m \times h}, \tag{7}$$

where $W^{(t)}$ and $B^{(t)}$ are the current hidden weights and bias matrix.

To provide supervision for gradient updates, a temporary output weight matrix $\Theta^{(t)}$ is computed in closed form by solving the ridge regression:

$$\Theta^{(t)} = \arg\min_{\Theta} \ \|H^{(t)}\Theta - Y\|_F^2 + \lambda\|\Theta\|_F^2. \tag{8}$$

The prediction $\hat{Y}^{(t)} = H^{(t)}\Theta^{(t)}$ is used to evaluate a squared error loss:

$$\mathcal{L}^{(t)} = \|\hat{Y}^{(t)} - Y\|_F^2, \tag{9}$$

which is backpropagated only through $W^{(t)}$ and $B^{(t)}$. This improves the alignment of the random features with the target signal, while keeping the training efficient since no backpropagation is applied to Θ. After T warm-up steps, the refined hidden weights are frozen, and final output weights are recomputed in closed form using the final hidden activations $H^{(T)}$.

3. **Closed-form Output Layer Learning:** Once the warm-up phase concludes, the updated hidden parameters $W^{(T)}$ and $B^{(T)}$ are frozen. The final hidden representation is computed as:

$$H = \phi(XW^{(T)} + B^{(T)}). \tag{10}$$

Then, the output weights $\Theta \in \mathbb{R}^{h \times n}$ are computed in closed form using regularized least squares:

$$\Theta = (H^\top H + \lambda I_h)^{-1} H^\top Y, \tag{11}$$

where I_h is the $h \times h$ identity matrix. This step is efficient and avoids iterative training, preserving the computational simplicity of RdNNs while benefiting from the improved feature representations produced during warm-up.

Algorithm 2 provides a detailed summary of the **`FLAiR`** framework, outlining the full warm-up and closed-form training procedure for input-to-hidden adaptation in RdNNs.

Remark 1. While the provided procedure presents **`FLAiR`** in the context of a shallow RdNN with a single hidden layer for notational clarity, the same principle extends seamlessly to deeper or structured RdNN architectures by applying the warm-up and freeze mechanism to each layer or subcomponent independently.

We further provide a formal result showing that the few-step supervised updates to the hidden parameters yield a monotonic *reduction in prediction loss* over warm-up epochs. This justifies the effectiveness of **`FLAiR`**'s adaptive initialization in aligning random features with the target task; see Lemma 3 in Appendix B. This result establishes a theoretical justification for **`FLAiR`**'s supervised warm-up strategy by demonstrating its guaranteed reduction in prediction error across gradient steps, thereby validating its role in improving hidden-layer alignment.

5 EMPIRICAL RESULTS

This section rigorously evaluates the effectiveness of the proposed **`StaR`** and **`FLAiR`** frameworks by integrating them into a diverse suite of representative RdNN architectures, encompassing shallow, multi-layer, and deep variant. Specifically, we consider Random Vector Functional Link Network (RVFL) Pao et al. (1994), Extreme Learning Machine (ELM) Huang et al. (2006), Broad Learning System (BLS) Chen & Liu (2017), and Deep Random Vector Functional Link Network (dRVFL) Shi et al. (2021). To assess the impact of proposed frameworks, we instantiate two distinct families of enhanced models:

- **`StaR`-enhanced RdNNs**: These variants apply the spectral regularization procedure of **`StaR`** to the randomly initialized weight matrices. The resulting models are denoted as **`StaR`**-RVFL, **`StaR`**-ELM, **`StaR`**-BLS, and **`StaR`**-dRVFL.
- **`FLAiR`-enhanced RdNNs**: These models incorporate the few-step adaptive initialization strategy of **`FLAiR`**. The corresponding enhanced variants are denoted as **`FLAiR`**-RVFL, **`FLAiR`**-ELM, **`FLAiR`**-BLS, and **`FLAiR`**-dRVFL.

The performance of these models is benchmarked against their baseline counterparts using a suite of statistical metrics and tests, including accuracy, standard deviation, rank analysis, Friedman test, Nemenyi posthoc test, and win-tie-loss analysis, ensuring a comprehensive and reliable analysis. The dataset description and detailed experimental setup is provided in Section C of the Appendix.

Dataset Description: The evaluation is conducted across 146 binary and multiclass benchmark datasets sourced from the UCI Dua & Graff (2017) and KEEL Derrac et al. (2015) repositories, ensuring robust generalization and diversity. Among the datasets, 93 are binary classification problems, and 53 are multiclass classification problems, with the number of classes ranging from 2 to 26. The number of samples spans from 16 to 130,064, and the number of features varies from 2 to 262, covering both small-scale and large-scale datasets as well as low-dimensional and high-dimensional data. For shallow (RVFL, ELM) and broad (BLS) architectures, along with their enhanced variants, all 146 datasets are utilized. In contrast, due to the higher computational complexity associated with training deep randomized models such as dRVFL and its enhanced counterparts, evaluation is conducted on a representative subset of 71 datasets (36 binary and 35 multiclass). The details of binary and multiclass datasets are provided in Section C of the Appendix.

5.1 PERFORMANCE EVALUATION AND ANALYSIS

We now present a detailed quantitative evaluation of the proposed **`StaR`** and **`FLAiR`** frameworks across 146 binary and multiclass classification datasets from various domains.

5.1.1 EFFECTIVENESS OF **`STAR`** FRAMEWORK

Tables 1a and 1b present the average accuracy, standard deviation, and rank statistics for the **`StaR`**-enhanced models (**`StaR`**-RVFL, **`StaR`**-ELM, **`StaR`**-BLS, and **`StaR`**-dRVFL) compared to their respective baselines on binary and multiclass datasets, respectively. The detailed results on each dataset are provided in the Section D of the Appendix. On binary classification datasets, for RVFL, **`StaR`** yields an absolute accuracy gain of 0.67% (from 85.13% to 85.80%) and reduces the standard deviation by 0.94 (from 5.87 to 4.93). In the case of ELM, **`StaR`** improves accuracy by 0.79% and

Table 1: Average performance comparison of baseline and **StaR**-enhanced RdNN models on (a) binary and (b) multiclass classification datasets. ↑ indicates improved accuracy (Acc.); ↓ denotes reduced standard deviation (Std.) and rank.

Model	**Acc.** ↑	**Std.** ↓	**Rank (Acc.)** ↓	**Rank (Std.)** ↓
RVFL	85.13	5.87	1.82	1.70
StaR-RVFL	**85.80** ↑	**4.93** ↓	**1.18** ↓	**1.30** ↓
ELM	84.98	5.82	1.77	1.71
StaR-ELM	**85.77** ↑	**4.98** ↓	**1.23** ↓	**1.29** ↓
BLS	85.60	5.31	1.83	1.69
StaR-BLS	**86.04** ↑	**4.56** ↓	**1.17** ↓	**1.31** ↓
dRVFL	83.13	6.84	1.97	1.97
StaR-dRVFL	**84.09** ↑	**5.34** ↓	**1.03** ↓	**1.03** ↓

(a) Binary datasets

Model	**Acc.** ↑	**Std.** ↓	**Rank (Acc.)** ↓	**Rank (Std.)** ↓
RVFL	77.29	8.80	1.82	1.85
StaR-RVFL	**78.01** ↑	**6.74** ↓	**1.18** ↓	**1.15** ↓
ELM	76.78	9.24	1.86	1.75
StaR-ELM	**77.88** ↑	**7.93** ↓	**1.14** ↓	**1.25** ↓
BLS	77.73	6.85	1.93	1.74
StaR-BLS	**78.53** ↑	**5.99** ↓	**1.07** ↓	**1.26** ↓
dRVFL	78.37	7.79	1.91	1.91
StaR-dRVFL	**79.37** ↑	**6.29** ↓	**1.09** ↓	**1.09** ↓

(b) Multiclass datasets

lowers variability by 0.84. BLS also benefits from **StaR**, showing a 0.44% increase in accuracy and a 0.75 reduction in standard deviation. Notably, dRVFL, despite being a deeper architecture, records the highest improvement in accuracy of 0.96%, along with a significant 1.50 decrease in standard deviation. Even greater gains are observed on multiclass classification datasets, where the benefits of integrating **StaR** become more prominent. For RVFL, the integration of **StaR** results in a notable accuracy improvement of 0.72% (from 77.29% to 78.01%) and a substantial 2.06 reduction in standard deviation, highlighting improved robustness across diverse class distributions. In the case of ELM, **StaR** provides a 1.10% boost in accuracy and a 1.31 decrease in variability, reinforcing its effectiveness even under higher output dimensionality. **StaR**-BLS achieves a 0.80% increase in accuracy and reduces the standard deviation by 0.86, showing enhanced stability. Once again, the deep architecture dRVFL benefits the most—registering the highest absolute accuracy gain of 1.00% and a 1.50 drop in standard deviation. These findings further affirm the consistent generalization and variance-reduction capabilities of **StaR**, especially in challenging multiclass scenarios. These empirical results strongly validate the theoretical foundations of the **StaR** framework. By constraining the spectral properties of random weight matrices, **StaR** enforces controlled transformations in the hidden layer, thereby mitigating noise amplification and improving stability across training runs. The observed improvements in both accuracy and standard deviation demonstrate that spectral regularization is an effective mechanism for enhancing generalization and reducing performance variability in RdNNs.

To further substantiate these findings, we analyze the average ranks based on accuracy and standard deviation, which jointly reflect generalization and stability across datasets. On binary classification tasks, all **StaR**-enhanced models exhibit lower ranks compared to their baselines. For instance, the accuracy rank of **StaR**-RVFL improves from 1.82 to 1.18, while its standard deviation rank improves from 1.70 to 1.30. Similarly, **StaR**-ELM and **StaR**-BLS reduce their accuracy ranks from 1.77 and 1.83 to 1.23 and 1.17, respectively, and their standard deviation ranks from 1.71 and 1.69 to 1.29 and 1.31. Notably, **StaR**-dRVFL achieves the best ranks in both dimensions: 1.03 for accuracy and 1.03 for standard deviation. These improvements are even more pronounced on multiclass datasets, where **StaR**-RVFL reduces its ranks from 1.82 and 1.85 to 1.18 and 1.15, respectively. Likewise, **StaR**-ELM achieves accuracy and stability ranks of 1.14 and 1.25, outperforming its baselines (1.86 and 1.75), while **StaR**-BLS improves from (1.93, 1.74) to (1.07, 1.26). Again, **StaR**-dRVFL delivers the most competitive ranking (1.09, 1.09), highlighting its effectiveness in high-dimensional, multi-class scenarios. These consistently lower ranks confirm the superior and robust performance of **StaR**-enhanced models across diverse datasets. Moreover, to statistically validate the observed improvements, we conduct multiple statistical tests, including the Friedman test, the Nemenyi posthoc test, and the win-tie-loss analysis Demšar (2006). The detailed results are provided in Section E of the Appendix.

5.1.2 EFFECTIVENESS OF **FLAiR** FRAMEWORK

Tables 2a and 2b summarize the average accuracy, standard deviation, and rank metrics for the **FLAiR**-enhanced models across binary and multiclass datasets. Detailed results for each dataset are included in Section *S.IV* of the supplement file. On binary classification tasks, **FLAiR**-RVFL improves accuracy by 1.44% (87.55% to 88.99%) and reduces the standard deviation by 0.79 (4.90

Table 2: Average performance comparison of baseline and **FLAiR**-enhanced RdNN models on (a) binary and (b) multiclass classification datasets. ↑ indicates improved accuracy (Acc.); ↓ denotes reduced standard deviation (Std.) and rank.

Model	Acc. ↑	Std. ↓	Rank (Acc.) ↓	Rank (Std.) ↓
RVFL	87.55	4.90	1.94	1.67
FLAiR-RVFL	**88.99** ↑	**4.11** ↓	**1.06** ↓	**1.33** ↓
ELM	87.49	4.71	1.95	1.71
FLAiR-ELM	**89.15** ↑	**3.68** ↓	**1.05** ↓	**1.29** ↓
BLS	86.75	3.99	1.96	1.65
FLAiR-BLS	**88.95** ↑	**3.39** ↓	**1.04** ↓	**1.35** ↓
dRVFL	83.13	6.84	1.96	1.90
FLAiR-dRVFL	**85.58** ↑	**4.49** ↓	**1.04** ↓	**1.10** ↓

(a) Binary datasets

Model	Acc. ↑	Std. ↓	Rank (Acc.) ↓	Rank (Std.) ↓
RVFL	79.47	6.86	1.99	1.61
FLAiR-RVFL	**81.39** ↑	**6.40** ↓	**1.01** ↓	**1.39** ↓
ELM	78.90	6.84	2.00	1.66
FLAiR-ELM	**81.43** ↑	**6.17** ↓	**1.00** ↓	**1.34** ↓
BLS	80.29	8.79	2.00	1.58
FLAiR-BLS	**83.56** ↑	**6.86** ↓	**1.00** ↓	**1.42** ↓
dRVFL	78.37	7.79	2.00	1.60
FLAiR-dRVFL	**81.51** ↑	**6.85** ↓	**1.00** ↓	**1.40** ↓

(b) Multiclass datasets

to 4.11). **FLAiR**-ELM shows an even larger gain of 1.66% in accuracy and a reduction of 1.03 in standard deviation. **FLAiR**-BLS improves accuracy by 2.20% and variability by 0.60. Notably, **FLAiR**-dRVFL records a substantial 2.45% increase in accuracy and a 2.35 drop in standard deviation, highlighting the framework's strong impact on deeper architectures. Performance gains are more pronounced in multiclass settings. **FLAiR**-RVFL improves accuracy by 1.92% and reduces standard deviation by 0.46. **FLAiR**-ELM exhibits a stronger gain, improving accuracy by 2.53% and reducing variability by 0.67. The highest accuracy improvement of 3.27% is achieved by **FLAiR**-BLS, which also shows a 1.93 decrease in standard deviation. **FLAiR**-dRVFL sees a 3.14% boost and a 0.94 drop in variability, confirming its ability to stabilize deep models in high-dimensional settings. These results empirically validate the core principle behind **FLAiR**: by briefly optimizing the input-to-hidden weights using gradient-based warm-up, **FLAiR** introduces task-specific structure into the initial random projections. This adaptive refinement aligns the hidden-layer transformations with the data distribution, thereby enhancing feature expressiveness and improves generalization performance across diverse architectures and tasks.

Rank-based evaluation further substantiates the superiority of **FLAiR**-enhanced models. On binary datasets, they achieve top accuracy ranks (1.04–1.06) and consistently lower standard deviation ranks (1.10–1.35), reflecting improved generalization and stability. On multiclass datasets, all models attain the best possible accuracy ranks (1.00–1.01), indicating that **FLAiR**-based models outperform their baselines across nearly every dataset. The corresponding drop in standard deviation ranks further confirms **FLAiR**'s ability to stabilize performance across varied classification tasks. Additional statistical significance test results (Friedman test, Nemenyi posthoc test, and win-tie-loss analysis) are provided in Section E of the Appendix.

Complementing these results, we empirically validate Lemma 3 by analyzing the progression of prediction loss over increasing warm-up epochs. As presented in Section F of the Appendix, the loss consistently exhibits a monotonic decline across multiple datasets, confirming that **FLAiR** effectively reduces prediction error through a few gradient updates of the input-to-hidden weights, thereby enhancing representational quality.

6 CONCLUSIONS

This work introduced two principled frameworks—**StaR** and **FLAiR**—that directly address the long-standing challenges of instability and weak representational capacity in randomized neural networks (RdNNs). **StaR** improves numerical stability by regulating the spectral characteristics of random weight matrices, while **FLAiR** enhances representational quality through lightweight, task-aware adaptation of fixed hidden-layer mappings. Rigorous theoretical analysis and comprehensive evaluations across 146 benchmark datasets validate the efficacy, stability, and generalization capabilities of both frameworks. Crucially, **StaR** and **FLAiR** are model-agnostic and can be seamlessly integrated into a wide range of RdNN architectures. We hope these contributions inspire further research for stabilizing and enriching randomized representations in modern neural learning. All implementation details, including code for baseline and **StaR**/**FLAiR**-enhanced models, are provided in the supplementary file.

REFERENCES

Jimmy Ba, Murat A Erdogdu, Taiji Suzuki, Zhichao Wang, Denny Wu, and Greg Yang. High-dimensional asymptotics of feature learning: How one gradient step improves the representation. *Advances in Neural Information Processing Systems*, 35:37932–37946, 2022.

Jiuwen Cao, Zhiping Lin, Guang-Bin Huang, and Nan Liu. Voting based extreme learning machine. *Information Sciences*, 185(1):66–77, 2012.

Weipeng Cao, Xizhao Wang, Zhong Ming, and Jinzhu Gao. A review on neural networks with random weights. *Neurocomputing*, 275:278–287, 2018.

Andrea Ceni. Random orthogonal additive filters: a solution to the vanishing/exploding gradient of deep neural networks. *IEEE Transactions on Neural Networks and Learning Systems*, 2025.

Chaofan Chen, Oscar Li, Daniel Tao, Alina Barnett, Cynthia Rudin, and Jonathan K Su. This looks like that: deep learning for interpretable image recognition. *Advances in Neural Information Processing Systems*, 32, 2019.

CL Philip Chen and Zhulin Liu. Broad learning system: An effective and efficient incremental learning system without the need for deep architecture. *IEEE Transactions on Neural Networks and Learning Systems*, 29(1):10–24, 2017.

Janez Demšar. Statistical comparisons of classifiers over multiple data sets. *The Journal of Machine Learning Research*, 7:1–30, 2006.

J Derrac, S Garcia, L Sanchez, and F Herrera. KEEL data-mining software tool: Data set repository, integration of algorithms and experimental analysis framework. *J. Mult. Valued Logic Soft Comput*, 17:255–287, 2015.

Dheeru Dua and Casey Graff. UCI machine learning repository. *URL http://archive. ics. uci. edu/ml*, 7(1):62, 2017.

Alan Edelman and N Raj Rao. Random matrix theory. *Acta Numerica*, 14:233–297, 2005.

Xavier Glorot and Yoshua Bengio. Understanding the difficulty of training deep feedforward neural networks. In *Proceedings of the thirteenth International Conference on Artificial Intelligence and Statistics*, pp. 249–256. JMLR Workshop and Conference Proceedings, 2010.

Gene H Golub and Charles F Van Loan. *Matrix computations*. JHU press, 2013.

Ian Goodfellow, Yoshua Bengio, Aaron Courville, and Yoshua Bengio. *Deep learning*, volume 1. MIT Press, 2016.

Li Guo, Runze Li, and Bin Jiang. An ensemble broad learning scheme for semisupervised vehicle type classification. *IEEE Transactions on Neural Networks and Learning Systems*, 32(12):5287–5297, 2021.

Minghui Hu, Ruobin Gao, and Ponnuthurai Nagaratnam Suganthan. Self-distillation for randomized neural networks. *IEEE Transactions on Neural Networks and Learning Systems*, 35(11):16119–16128, 2024.

Guang-Bin Huang, Qin-Yu Zhu, and Chee-Kheong Siew. Extreme learning machine: theory and applications. *Neurocomputing*, 70(1-3):489–501, 2006.

Boris Igelnik and Yoh-Han Pao. Stochastic choice of basis functions in adaptive function approximation and the functional-link net. *IEEE Transactions on Neural Networks*, 6(6):1320–1329, 1995.

Ronald L Iman and James M Davenport. Approximations of the critical region of the fbietkan statistic. *Communications in Statistics-Theory and Methods*, 9(6):571–595, 1980.

Ajay Jaiswal, Peihao Wang, Tianlong Chen, Justin Rousseau, Ying Ding, and Zhangyang Wang. Old can be gold: Better gradient flow can make vanilla-gcns great again. In *Advances in Neural Information Processing Systems*, volume 35, pp. 7561–7574, 2022.

Diederik P. Kingma and Jimmy Ba. Adam: A method for stochastic optimization, 2017. URL `https://arxiv.org/abs/1412.6980`.

Ivano Lauriola, Alberto Lavelli, and Fabio Aiolli. An introduction to deep learning in natural language processing: Models, techniques, and tools. *Neurocomputing*, 470:443–456, 2022.

Yann LeCun, Yoshua Bengio, and Geoffrey Hinton. Deep learning. *Nature*, 521(7553):436–444, 2015.

Ming Li and Dianhui Wang. Insights into randomized algorithms for neural networks: Practical issues and common pitfalls. *Information Sciences*, 382:170–178, 2017.

Yicheng Liu, Jie Wen, Chengliang Liu, Xiaozhao Fang, Zuoyong Li, Yong Xu, and Zheng Zhang. Language-driven cross-modal classifier for zero-shot multi-label image recognition. In *Proceedings of the 41st International Conference on Machine Learning*, volume 235, pp. 32173–32183, 2024.

Bingjun Luo, Junjie Zhu, Tianyu Yang, Sicheng Zhao, Chao Hu, Xibin Zhao, and Yue Gao. Learning deep hierarchical features with spatial regularization for one-class facial expression recognition. In *Proceedings of the AAAI Conference on Artificial Intelligence*, volume 37, pp. 6065–6073, 2023.

Takeru Miyato, Toshiki Kataoka, Masanori Koyama, and Yuichi Yoshida. Spectral normalization for generative adversarial networks. *arXiv preprint arXiv:1802.05957*, 2018.

Deanna Needell, Aaron A Nelson, Rayan Saab, Palina Salanevich, and Olov Schavemaker. Random vector functional link networks for function approximation on manifolds. *Frontiers in Applied Mathematics and Statistics*, 10:1284706, 2024.

Daniel W. Otter, Julian R. Medina, and Jugal K. Kalita. A survey of the usages of deep learning for natural language processing. *IEEE Transactions on Neural Networks and Learning Systems*, 32 (2):604–624, 2021. doi: 10.1109/TNNLS.2020.2979670.

Yoh-Han Pao, Gwang-Hoon Park, and Dejan J Sobajic. Learning and generalization characteristics of the random vector functional-link net. *Neurocomputing*, 6(2):163–180, 1994.

Razvan Pascanu, Tomas Mikolov, and Yoshua Bengio. On the difficulty of training recurrent neural networks. In *Proceedings of the 30th International Conference on Machine Learning*, volume 28 of *Proceedings of Machine Learning Research*, pp. 1310–1318, 2013.

M. Sajid, A. K. Malik, and M. Tanveer. Intuitionistic fuzzy broad learning system: Enhancing robustness against noise and outliers. *IEEE Transactions on Fuzzy Systems*, 32(8):4460–4469, 2024a. doi: 10.1109/TFUZZ.2024.3400898.

M. Sajid, A. K. Malik, M. Tanveer, and Ponnuthurai N. Suganthan. Neuro-fuzzy random vector functional link neural network for classification and regression problems. *IEEE Transactions on Fuzzy Systems*, 32(5):2738–2749, 2024b.

M Sajid, A Quadir, M Tanveer, and for the Alzheimer's Disease Neuroimaging Initiative. GB-RVFL: Fusion of randomized neural network and granular ball computing. *Pattern Recognition*, 159:111142, 2025a.

M. Sajid, M. Tanveer, and Ponnuthurai N. Suganthan. Ensemble deep random vector functional link neural network based on fuzzy inference system. *IEEE Transactions on Fuzzy Systems*, 33(1): 479–490, 2025b.

Andrew M Saxe, James L McClelland, and Surya Ganguli. Exact solutions to the nonlinear dynamics of learning in deep linear neural networks. *arXiv preprint arXiv:1312.6120*, 2013.

Simone Scardapane and Dianhui Wang. Randomness in neural networks: an overview. *Wiley Interdisciplinary Reviews: Data Mining and Knowledge Discovery*, 7(2):e1200, 2017.

Qiushi Shi, Rakesh Katuwal, Ponnuthurai N Suganthan, and Muhammad Tanveer. Random vector functional link neural network based ensemble deep learning. *Pattern Recognition*, 117:107978, 2021.

Ponnuthurai N Suganthan and Rakesh Katuwal. On the origins of randomization-based feedforward neural networks. *Applied Soft Computing*, 105:107239, 2021.

T Tao. Topics in random matrix theory. american mathematical society. *Graduate Studies in Mathematics*, 132, 2012. URL `https://doi.org/10.1090/gsm/132`.

Rishabh Tiwari, Arnav Chavan, Deepak Gupta, Gowreesh Mago, Animesh Gupta, Akash Gupta, Suraj Sharan, Yukun Yang, Shanwei Zhao, Shihao Wang, et al. Rcv2023 challenges: Benchmarking model training and inference for resource-constrained deep learning. In *Proceedings of the IEEE/CVF International Conference on Computer Vision*, pp. 1534–1543, 2023.

Athanasios Voulodimos, Nikolaos Doulamis, Anastasios Doulamis, and Eftychios Protopapadakis. Deep learning for computer vision: A brief review. *Computational Intelligence and Neuroscience*, 2018(1):7068349, 2018.

Fan Yin, Jayanth Srinivasa, and Kai-Wei Chang. Characterizing truthfulness in large language model generations with local intrinsic dimension. In *Proceedings of the 41st International Conference on Machine Learning*, volume 235, pp. 57069–57084, 2024.

Jiong Zhang, Qi Lei, and Inderjit Dhillon. Stabilizing gradients for deep neural networks via efficient svd parameterization. In *International Conference on Machine Learning*, pp. 5806–5814. PMLR, 2018.

Le Zhang and Ponnuthurai N Suganthan. A survey of randomized algorithms for training neural networks. *Information Sciences*, 364:146–155, 2016.

Yongshan Zhang, Jia Wu, Zhihua Cai, Bo Du, and S Yu Philip. An unsupervised parameter learning model for rvfl neural network. *Neural Networks*, 112:85–97, 2019.

APPENDIX

A ARCHITECTURAL AND MATHEMATICAL FORMULATION OF STANDARD RDNN MODELS

A.1 FORMULATION AND ARCHITECTURE OF RVFL AND ELM PAO ET AL. (1994); HUANG ET AL. (2006)

RVFL and ELM are single-layer feed-forward RdNNs that rely on hidden layer transformations and closed-form solutions for output weight computation. While their architectures share significant similarities, the primary distinction lies in the presence of direct input-to-output connections in RVFL, which are absent in ELM. Their common formulation is described as follows:
Hidden Layer: The hidden layer transforms the input data X using a random weight matrix $W \in \mathbb{R}^{d\times h}$ and bias $B \in \mathbb{R}^{m\times h}$:

$$H = \phi(XW + B), \tag{12}$$

where $\phi(\cdot)$ is the non-linear function and h represents the number of nodes in the hidden layer.
Output Layer: In RVFL, the final output combines the hidden layer outputs and the original inputs to form an augmented representation:

$$A = [X \mid H], \tag{13}$$

whereas in ELM, the output is directly derived from the hidden layer outputs:

$$A = H. \tag{14}$$

The output weight matrix $\Theta \in \mathbb{R}^{h\times n_{\text{class}}}$ is computed in both architectures using a closed-form solution:

$$\Theta = (A^\top A + \lambda I)^{-1} A^\top Y, \tag{15}$$

where λ is a regularization parameter.

Key Difference: RVFL incorporates direct input-to-output connections ($Z = [X \mid H]$), which preserve input information and enhance robustness. In contrast, ELM omits this feature ($Z = H$), resulting in a simpler architecture that trades off some robustness for faster training.

A.2 FORMULATION AND ARCHITECTURE OF BLS CHEN & LIU (2017)

BLS represents a significant advancement in RdNNs by utilizing a flat architecture instead of the deep hierarchical structures seen in traditional deep learning. The architecture of BLS consists of three primary components: the feature layer, the enhancement layer, and the output layer. The feature layer is responsible for extracting meaningful features from the input data by generating multiple groups of feature nodes through random projection and non-linear transformations. On the other hand, the enhancement layer enriches the feature representations by applying additional non-linear transformations, thereby constructing enhancement nodes that provide diversity and robustness. The outputs from both layers are concatenated to form a final matrix, which is used to compute the output weights via a closed-form solution. Its architecture can be described as follows:
Feature Layer: For the input matrix X, the feature layer generates q windows of feature nodes. Each window f_i contains p nodes, which are computed as:

$$Z_{f_i} = \phi(XW_{f_i} + B_{f_i}), \tag{16}$$

where $W_{f_i} \in \mathbb{R}^{d\times p}$ is a random weight matrix, $B_{f_i} \in \mathbb{R}^{m\times p}$ is a bias matrix, $\phi(\cdot)$ is a non-linear function, and $Z_{f_i} \in \mathbb{R}^{m\times p}$ represents the output of the i^{th} feature node window. The outputs of all feature windows are concatenated to form the overall feature layer output:

$$Z = [Z_{f_1}, Z_{f_2}, \dots, Z_{f_q}], \tag{17}$$

where $Z \in \mathbb{R}^{m\times pq}$. The feature layer output Z serves as the input to the enhancement layer.
Enhancement Layer: The enhancement layer enriches the feature representation by applying additional random transformations and a non-linear function to the concatenated feature nodes Z. Each window (e_j) of enhancement nodes (there are s windows, each with r nodes) is computed as:

$$E_{e_j} = \psi(ZW_{e_j} + B_{e_j}), \tag{18}$$

where $Z \in \mathbb{R}^{m\times pq}$ is the output from the feature layer, $W_{e_j} \in \mathbb{R}^{pq\times r}$ is a random weight matrix, $B_{e_j} \in \mathbb{R}^{m\times r}$ is a bias matrix, $\psi(\cdot)$ is a non-linear function, and $E_{e_j} \in \mathbb{R}^{m\times r}$ is the output of the j^{th} enhancement node window. The outputs of all enhancement windows are concatenated to form the overall enhancement layer output:

$$E = [E_{e_1}, E_{e_2}, \ldots, E_{e_s}], \tag{19}$$

where $E \in \mathbb{R}^{m\times rs}$.

Output Layer: The final representation matrix A, which combines the outputs of the feature and enhancement layers, is given by:

$$A = [Z \,|\, E], \tag{20}$$

where $A \in \mathbb{R}^{m\times(pq+rs)}$.

The output weights $\Theta \in \mathbb{R}^{(pq+rs)\times n_{\text{class}}}$ are then learned using a closed-form solution:

$$\Theta = (A^\top A + \lambda I)^{-1} A^\top Y, \tag{21}$$

where λ is a regularization parameter.

Incremental Learning: One of BLS's unique features is its ability to incrementally update the network by adding new feature mapping nodes or enhancement nodes without retraining the entire model. This makes BLS computationally efficient and adaptable to streaming or evolving data.

A.3 FORMULATION AND ARCHITECTURE OF DEEP RVFL SHI ET AL. (2021)

The deep random vector functional link network (dRVFL) extends the standard RVFL architecture by incorporating multiple hidden layers, thereby enhancing its representational capacity while preserving the hallmark efficiency of closed-form training. Unlike conventional deep neural networks, dRVFL stacks several RVFL-like layers where only the final layer's output weights are trained via least squares, and all intermediate transformations are computed using fixed, randomly initialized weights. The architecture can be described as follows:

Layer-wise Random Transformations: Let the input matrix be $X \in \mathbb{R}^{m\times d}$. The l^{th} hidden layer transformation is defined as:

$$H^{(l)} = \phi(H^{(l-1)} W^{(l)} + B^{(l)}), \quad l = 1, 2, \ldots, L, \tag{22}$$

where $H^{(0)} = X$, $W^{(l)} \in \mathbb{R}^{h_{l-1}\times h_l}$ is the randomly initialized weight matrix for layer l, $B^{(l)} \in \mathbb{R}^{m\times h_l}$ is the corresponding bias matrix, and $\phi(\cdot)$ is a nonlinear activation function applied elementwise.

Augmented Feature Representation: The final feature representation A is constructed by concatenating the original input and the outputs of all hidden layers:

$$A = [X \,|\, H^{(1)} \,|\, H^{(2)} \,|\, \ldots \,|\, H^{(L)}] \in \mathbb{R}^{m\times a} \tag{23}$$

where $a = d + \sum_{l=1}^{L} h_l$ is the total feature dimensionality. This dense aggregation of features enables dRVFL to capture increasingly abstract representations at deeper layers while retaining the original input.

Output Layer: The output weights $\Theta \in \mathbb{R}^{a\times n_{\text{class}}}$ are obtained using the same closed-form solution as in RVFL:

$$\Theta = (A^\top A + \lambda I)^{-1} A^\top Y, \tag{24}$$

where $\lambda \geq 0$ is the regularization parameter.

B THEORETICAL ANALYSIS

Lemma 1 (Spectral Conditioning via **`StaR`**). *Let $W \in \mathbb{R}^{d\times h}$ be a randomly initialized weight matrix with singular value decomposition $W = U\Sigma V^\top$, and let $W' = U\Sigma' V^\top$ be the spectrally regulated matrix obtained via the **`StaR`** procedure, where each singular value $\sigma'_i \in [\sigma_{low}, \sigma_{high}]$ for fixed bounds $0 < \sigma_{low} < \sigma_{high}$. Then, the regulated matrix W' satisfies:*

1. *Spectral norm:* $\|W'\|_2 \le \sigma_{high}$,
2. *Minimal singular value:* $\sigma_{\min}(W') \ge \sigma_{low}$,
3. *Condition number:* $\kappa(W') = \frac{\|W'\|_2}{\sigma_{\min}(W')} \le \frac{\sigma_{high}}{\sigma_{low}}$.

Proof. By construction, the **StaR** framework rescales the singular values $\{\sigma_i\}$ of W to lie within the interval $[\sigma_{\text{low}}, \sigma_{\text{high}}]$. Therefore, the resulting matrix $\Sigma' = \text{diag}(\sigma_1', \ldots, \sigma_r')$ satisfies:

$$\sigma_{\min}(W') = \min_i \sigma_i' \ge \sigma_{\text{low}}, \quad \sigma_{\max}(W') = \max_i \sigma_i' \le \sigma_{\text{high}}.$$

Hence, the operator norm $\|W'\|_2 = \sigma_{\max}(W') \le \sigma_{\text{high}}$, and the condition number $\kappa(W') = \frac{\sigma_{\max}}{\sigma_{\min}} \le \frac{\sigma_{\text{high}}}{\sigma_{\text{low}}}$, which completes the proof. $\square$

Lemma 2 (Lipschitz Stability of the **StaR**-Transformed Mapping)**.** *Let $\phi : \mathbb{R} \to \mathbb{R}$ be an L_ϕ-Lipschitz activation function applied elementwise, and let $W' \in \mathbb{R}^{d\times h}$ be a **StaR**-regularized weight matrix satisfying $\|W'\|_2 \le \sigma_{high}$. Then the hidden transformation $X \mapsto \phi(XW' + B)$ is Lipschitz continuous with constant $L_\phi \cdot \sigma_{high}$, i.e.,*

$$\|\phi(X_1W' + B) - \phi(X_2W' + B)\|_F \le L_\phi \cdot \sigma_{high} \cdot \|X_1 - X_2\|_F$$

for all $X_1, X_2 \in \mathbb{R}^{m\times d}$ and fixed bias matrix $B \in \mathbb{R}^{m\times h}$.

Proof. By the Lipschitz continuity of ϕ, applied elementwise,

$$\|\phi(X_1W' + B) - \phi(X_2W' + B)\|_F \le L_\phi \cdot \|(X_1 - X_2)W'\|_F.$$

Using the submultiplicativity of the Frobenius norm:

$$\|(X_1 - X_2)W'\|_F \le \|X_1 - X_2\|_F \cdot \|W'\|_2.$$

Since **StaR** ensures $\|W'\|_2 \le \sigma_{\text{high}}$, we obtain:

$$\|\phi(X_1W' + B) - \phi(X_2W' + B)\|_F \le L_\phi \cdot \sigma_{\text{high}} \cdot \|X_1 - X_2\|_F,$$

which concludes the proof. $\square$

Lemma 3 (Supervised Warm-up Improves Output Prediction)**.** *Let $H^{(0)} = \phi(XW^{(0)} + B^{(0)}) \in \mathbb{R}^{m\times h}$ be the initial hidden representation obtained from randomly initialized weights and biases, and let $\Theta^{(0)}$ be the corresponding closed-form output weights:*

$$\Theta^{(0)} = \arg\min_\Theta \|H^{(0)}\Theta - Y\|_F^2 + \lambda\|\Theta\|_F^2.$$

*Suppose that during the warm-up phase of **FLAiR**, the weights W and biases B are updated for T steps using the loss*

$$\mathcal{L}^{(t)} = \|H^{(t)}\Theta^{(t)} - Y\|_F^2,$$

where $H^{(t)} = \phi(XW^{(t)} + B^{(t)})$ and $\Theta^{(t)}$ is the closed-form solution at step t. Then, under the assumption that ϕ is differentiable and updates are performed using gradient descent with sufficiently small step size, the final prediction error after warm-up satisfies:

$$\|H^{(T)}\Theta^{(T)} - Y\|_F^2 \le \|H^{(0)}\Theta^{(0)} - Y\|_F^2.$$

Proof. At each warm-up step t, the output weights $\Theta^{(t)}$ are computed as the minimizer of the regularized least squares problem:

$$\Theta^{(t)} = (H^{(t)\top}H^{(t)} + \lambda I_h)^{-1}H^{(t)\top}Y.$$

The loss function minimized via backpropagation is:

$$\mathcal{L}^{(t)} = \|H^{(t)}\Theta^{(t)} - Y\|_F^2.$$

The gradient descent step on $W^{(t)}$, $B^{(t)}$ aims to reduce this loss at every iteration. Under standard smoothness assumptions on ϕ (e.g., Lipschitz continuity of its gradient), and for small enough learning rate, gradient descent ensures monotonic decrease in the training loss:

$$\mathcal{L}^{(t+1)} \leq \mathcal{L}^{(t)}, \quad \forall t.$$

Thus, by induction over T steps, we obtain:

$$\mathcal{L}^{(T)} \leq \mathcal{L}^{(0)}.$$

Since $\mathcal{L}^{(t)} = \|H^{(t)}\Theta^{(t)} - Y\|_F^2$, this yields the desired result:

$$\|H^{(T)}\Theta^{(T)} - Y\|_F^2 \leq \|H^{(0)}\Theta^{(0)} - Y\|_F^2.$$

□

C EXPERIMENTAL SETUP AND HYPERPARAMETER SETTING

Experimental Setup: All experiments for the baseline RVFL, ELM, and BLS models, along with their **`StaR`**-enhanced counterparts, are implemented using MATLAB R2023a and executed on a Windows 10 PC equipped with an Intel(R) Core(TM) i7-6700 CPU @ 3.40GHz (4 cores, 8 logical processors) and 16 GB RAM. The dRVFL model and its **`StaR`**-enhanced version, as well as all **`FLAiR`**-enhanced models and their corresponding baselines, are implemented in Python 3.12.7 within a Conda environment (version 24.11.3) and executed using Visual Studio Code on the same hardware configuration. Each dataset is preprocessed by normalizing the input features to have zero mean and unit variance. The details of all binary and multiclass datasets used in the experiments are provided in Table 3. A 5-fold cross-validation procedure is employed to ensure reliable and unbiased evaluation. In each fold, the dataset is split into 80% training data and 20% testing data. For every combination of hyperparameters, the model is trained on the training data and evaluated on the testing data across all 5 folds. The testing accuracy is recorded for each fold. The final testing accuracy for each dataset is computed as the mean testing accuracy across the five folds, providing a robust estimate of the model's performance. Additionally, the standard deviation of testing accuracy across the folds is recorded to quantify the stability of the model.

Hyperparameter Setting: Hyperparameter tuning is performed using a grid search strategy to identify the optimal settings for each model. For each model, the regularization parameter (λ) is selected from $\{10^i \mid i = -5, -4, \ldots, 5\}$. For RVFL and ELM, the number of hidden nodes (h) varies from $[3 : 20 : 203]$, and six activation functions (Sigmoid (1), Sine (2), Tribas (3), Radbas (4), Tansig (5), and ReLU (6)) are evaluated. For BLS, the number of feature windows (q), the number of feature nodes in each window (p), and the number of enhancement nodes (r) are set as per Sajid et al. (2024a), with Tansig as the activation function. For dRVFL, we adopt the same hyperparameter settings as provided in Shi et al. (2021) and evaluate three activation functions: Sigmoid (1), ReLU (2), and SELU (3). For the **`StaR`**-enhanced counterparts, the spectral bounds are selected by varying the upper threshold σ_{high} in the range $\{0.5, 0.75, 1.0, 1.25, 1.5, 1.75, 2.0\}$, with the corresponding lower bound set as $\sigma_{\text{low}} = 0.1 \cdot \sigma_{\text{high}}$. For the **`FLAiR`**-enhanced counterparts, the number of warm-up epochs is chosen from the range $\{2, 3, \ldots, 10\}$, enabling progressive refinement of the input-to-hidden weights via lightweight adaptation. All **`FLAiR`** models are trained using the standard Adam optimizer Kingma & Ba (2017) for backpropagation during the warm-up phase.

D DATASET-WISE RESULTS ON BINARY AND MULTICLASS DATASETS

The experimental results are comprehensively summarized in Tables 4 - 9. Tables 4 and 5 compare the baseline RVFL, ELM, and BLS models with their **`StaR`**-enhanced counterparts on binary and multiclass classification tasks, respectively. Tables 6 and 7 present similar comparisons for the **`FLAiR`**-enhanced versions. Furthermore, Tables 8 and 9 provide the performance of dRVFL and its enhancements using both the **`StaR`** and **`FLAiR`** frameworks on binary and multiclass datasets, respectively.

E STATISTICAL ANALYSIS

To statistically validate the observed improvements, we conduct multiple statistical tests, including the Friedman test, the Nemenyi post-hoc test, and the win–tie–loss analysis Demšar (2006).

Table 3: Summary of all datasets used in the experiments. The table lists the dataset name, number of samples, number of features, and number of classes.

Dataset	**Number of Samples**	**Number of Features**	**Number of Classes**	**Dataset**	**Number of Samples**	**Number of Features**	**Number of Classes**
Binary datasets							
acute_inflammation	120	6	2	monk2	601	7	2
acute_nephritis	120	6	2	monk3	554	6	2
balloons	16	4	2	new-thyroid1	215	5	2
fertility	100	9	2	pima	768	8	2
parkinsons	195	22	2	ripley	1250	2	2
pittsburg_bridges_T_OR_D	102	7	2	segment0	2308	19	2
bank	4521	16	2	shuttle-6_vs_2-3	230	9	2
blood	748	4	2	shuttle-c0-vs-c4	1829	9	2
breast_cancer	286	9	2	sonar	208	60	2
breast_cancer_wisc	699	9	2	votes	435	16	2
breast_cancer_wisc_diag	569	30	2	vowel	988	10	2
breast_cancer_wisc_prog	198	33	2	wpbc	194	33	2
chess_krvkp	3196	36	2	yeast-0-2-5-6_vs_3-7-8-9	1004	8	2
congressional_voting	435	16	2	yeast-0-2-5-7-9_vs_3-6-8	1004	8	2
conn_bench_sonar_mines_rocks	208	60	2	yeast-0-5-6-7-9_vs_4	528	8	2
credit_approval	690	15	2	yeast-2_vs_4	514	8	2
cylinder_bands	512	35	2	yeast1vs7	459	8	2
echocardiogram	131	10	2	yeast2vs8	483	8	2
haberman_survival	306	3	2	yeast3	1484	8	2
hepatitis	155	19	2	**Dataset**	**Number of Samples**	**Number of Features**	**Number of Classes**
horse_colic	368	25	2	**Multiclass Dataset**			
ilpd_indian_liver	583	9	2	abalone	4177	8	3
ionosphere	351	33	2	annealing	898	31	5
monks_1	556	6	2	arrhythmia	452	262	13
monks_3	554	6	2	balance_scale	625	4	3
oocytes_merluccius_nucleus_4d	1022	41	2	cardiotocography_10clases	2126	21	10
oocytes_trisopterus_nucleus_2f	912	25	2	cardiotocography_3clases	2126	21	3
pima	768	8	2	conn_bench_vowel_deterding	990	11	11
planning	182	12	2	contrac	1473	9	3
spect	265	22	2	dermatology	366	34	6
spectf	267	44	2	ecoli	336	7	8
statlog_australian_credit	690	14	2	energy_y1	768	8	3
statlog_german_credit	1000	24	2	energy_y2	768	8	3
statlog_heart	270	13	2	flags	194	28	8
tic_tac_toe	958	9	2	glass	214	9	6
titanic	2201	3	2	heart_cleveland	303	13	5
adult	48842	14	2	heart_switzerland	123	12	5
connect_4	67557	42	2	image_segmentation	2310	18	7
hill_valley	1212	100	2	iris	150	4	3
magic	19020	10	2	led_display	1000	7	10
miniboone	130064	50	2	lenses	24	4	3
mushroom	8124	21	2	letter	20000	16	26
musk_2	6598	166	2	low_res_spect	531	100	9
ozone	2536	72	2	lymphography	148	18	4
spambase	4601	57	2	molec_biol_splice	3190	60	3
twonorm	7400	20	2	nursery	12960	8	5
abalone9-18	731	7	2	oocytes_merluccius_states_2f	1022	25	3
aus	690	14	2	oocytes_trisopterus_states_5b	912	32	3
brwisconsin	683	9	2	optical	5620	62	10
bupa or liver-disorders	345	6	2	page_blocks	5473	10	5
checkerboard_Data	690	14	2	pendigits	10992	16	10
cleve	297	13	2	pittsburg_bridges_MATERIAL	106	7	3
crossplane150	150	2	2	pittsburg_bridges_REL_L	103	7	3
ecoli-0-1-4-6_vs_5	280	6	2	pittsburg_bridges_SPAN	92	7	3
ecoli-0-1-4-7_vs_2-3-5-6	336	7	2	pittsburg_bridges_TYPE	105	7	6
ecoli-0-1_vs_2-3-5	244	7	2	post_operative	90	8	3
ecoli-0-1_vs_5	240	6	2	seeds	210	7	3
ecoli-0-2-3-4_vs_5	202	7	2	semeion	1593	256	10
ecoli-0-2-6-7_vs_3-5	224	7	2	soybean	683	35	18
ecoli-0-3-4-6_vs_5	205	7	2	statlog_image	2310	18	7
ecoli-0-3-4-7_vs_5-6	257	7	2	statlog_landsat	6435	36	6
ecoli-0-4-6_vs_5	203	6	2	statlog_shuttle	58000	9	7
ecoli-0-6-7_vs_5	220	6	2	statlog_vehicle	846	18	4
ecoli0137vs26	311	7	2	synthetic_control	600	60	6
ecoli01vs5	240	7	2	thyroid	7200	21	3
ecoli3	336	7	2	vertebral_column_3clases	310	6	3
ecoli4	336	7	2	wall_following	5456	24	4
glass2	214	9	2	waveform	5000	21	3
haber	306	3	2	waveform_noise	5000	40	3
haberman	306	3	2	wine	178	13	3
heart-stat	270	13	2	wine_quality_red	1599	11	6
iono	351	33	2	wine_quality_white	4898	11	7
led7digit-0-2-4-5-6-7-8-9_vs_1	443	7	2	yeast	1484	8	10
monk1	556	6	2	zoo	101	16	7

The Friedman test results, presented in Tables 10 and 11, confirm that the StaR- and FLAiR-enhanced models consistently achieve statistically significant improvements over their respective baselines. According to the null hypothesis, all models are considered equivalent, implying that their average ranks do not significantly differ. The Friedman test statistic, which adheres to a chi-squared (χ_F^2) distribution with $l-1$ degrees of freedom (where l represents the total number of models), is computed as $\chi_F^2 = \frac{12\mathcal{D}}{l(l+1)}\left[\sum_k R_k^2 - \frac{l(l+1)^2}{4}\right]$, where $\mathcal{D}$ represents the number of datasets, and R_k denotes the mean rank of the k^{th} model. Since the Friedman statistic is often overly conservative, an improved statistic proposed by Iman & Davenport (1980) provides a more accurate measure: $F_F = \frac{(\mathcal{D}-1)\chi_F^2}{\mathcal{D}(l-1)-\chi_F^2}$, which follows the F-distribution with degrees of freedom $(l-1)$ and $(l-1)(\mathcal{D}-1)$. At a 5% significance level, the critical values of $F((l-1),(l-1)(\mathcal{D}-1))$ are obtained from the F-distribution table. For RVFL, ELM, and BLS, the critical values are 3.94455 for binary datasets and 4.0266 for multi-class datasets. For dRVFL, the corresponding critical values are 4.1213 and 4.13, respectively. Since $F_F > F((l-1),(l-1)(\mathcal{D}-1))$ for all cases, the null hypothesis is rejected, confirming that the performance differences among the models are statistically significant.

Table 4: Comparison of RVFL, ELM, and BLS with their **`StaR`**-enhanced counterparts on binary classification tasks.

Dataset	RVFL		**`StaR`**-RVFL		ELM		**`StaR`**-ELM		BLS		**`StaR`**-BLS	
	Acc.	Std.	Acc.	Std.	Acc.	Std.	Acc.	Std.	Acc.	Std.	Acc.	Std.
acute_nephritis	100	0	100	0	100	0	100	0	100	0	100	0
balloons	75	14.4338	86.6667	19.8142	73.3333	27.8887	86.6667	18.2574	86.6667	18.2574	86.6667	11.2574
fertility	91	8.2158	91	8.2158	91	8.2158	91	8.2158	90	10	91	8.2158
parkinsons	83.0769	12.8972	84.1026	10.7875	82.0513	17.6719	83.5897	17.4472	81.5385	16.3581	84.6154	10.4154
pittsburg_bridges_T_OR_D	88.2381	8.9271	91.1905	3.9912	87.2381	10.261	90.1905	4.8894	91.1905	6.3976	90.1905	6.1293
bank	89.6926	0.4758	89.936	0.5773	89.5377	0.3955	89.9139	0.3463	89.7809	0.4067	90.0905	0.6165
blood	76.5056	13.5754	77.7047	12.4533	76.7723	13.3533	77.4371	12.5572	77.9723	11.6847	78.1065	10.793
breast_cancer	70.1754	44.6249	70.1754	32.4134	70.1754	44.6249	70.1754	32.2805	70.2057	26.0229	73.3333	22.3932
breast_cancer_wisc	88.4183	6.7943	88.9866	4.297	88.4152	3.6106	89.1305	3.076	88.1336	5.2028	88.4193	4.9471
breast_cancer_wisc_diag	94.549	2.5218	95.6078	1.7506	94.0273	1.8937	95.2538	2.2902	94.3798	3.2536	94.5536	2.7283
breast_cancer_wisc_prog	81.3846	8.341	82.359	5.2159	80.8974	9.027	82.8718	4.3114	83.3846	8.4335	81.3846	7.0594
chess_krvkp	81.6346	7.0558	83.1976	4.8692	80.4456	6.8631	82.3852	5.4534	85.2316	4.0604	85.0434	3.1451
congressional_voting	63.4483	4.9036	63.908	2.5183	62.9885	4.0962	64.1379	3.4864	63.6782	2.885	64.3678	3.8084
conn_bench_sonar_mines_rocks	60.1161	12.8152	64.4019	2.9293	62.5436	8.566	63.4262	6.2516	68.3391	9.7684	71.1614	6.0878
credit_approval	85.3623	12.1838	85.6522	10.355	85.0725	11.4415	85.7971	8.8542	86.6667	10.3702	87.1014	9.125
cylinder_bands	67.5919	5.0677	70.3122	5.2431	67.7803	3.7032	69.9277	2.536	69.5298	3.8847	69.9219	3.4197
echocardiogram	84.6724	7.2724	85.4416	6.3987	84.7009	5.5176	86.2108	7.0505	85.4416	6.3987	85.4416	6.4657
haberman_survival	73.4902	8.4751	73.4902	8.4751	73.4902	8.4751	73.8181	8.4202	70.6029	6.662	73.4902	8.4751
hepatitis	84.5161	12.7817	85.1613	8.7156	83.2258	9.2373	86.4516	8.0467	85.1613	10.6011	85.8065	9.8374
horse_colic	86.1385	3.7694	86.4198	3.281	86.4235	4.9395	86.6753	2.6833	86.6938	3.1932	87.2381	3.7511
ilpd_indian_liver	71.7138	6.9558	72.903	4.2655	71.8744	4.0378	71.8671	5.5082	72.0395	4.6401	72.9016	5.5345
ionosphere	90.33	5.7816	90.6278	6.9368	89.7626	6.0272	90.6117	5.7258	88.3541	9.5467	89.2032	8.634
monks_1	81.6297	13.7116	83.4363	8.6492	83.7902	9.1321	82.7107	9.1082	74.6268	5.3631	76.6007	4.4489
monks_3	91.1581	4.0925	91.8804	3.8683	90.9812	4.3104	92.0622	5.3771	87.5414	4.6258	87.1957	5.9057
oocytes_merluccius_nucleus_4d	82.5868	3.0751	83.66	2.9505	82.0937	3.1457	83.3649	1.9663	82.4859	2.1099	83.0722	1.8323
oocytes_trisopterus_nucleus_2f	79.2686	4.1506	80.9127	5.4171	78.5096	3.8063	80.5855	3.3711	78.9443	2.073	80.0408	2.6117
pima	72.532	4.4896	75.0055	3.9788	73.0473	1.4865	74.4843	2.5672	72.2655	3.8872	72.5236	3.2635
planning	71.3814	8.8534	71.9369	8.2169	71.9369	9.2169	71.9369	7.1382	71.3814	8.8534	73.5886	7.1156
spect	67.9245	7.893	68.6792	3.1572	67.9245	6.3984	68.3019	3.3752	69.0566	4.1338	69.8113	4.2243
spectf	79.3431	20.8936	79.3431	20.8936	79.7205	20.7374	79.3431	16.8936	79.3431	20.8936	79.7205	20.7374
statlog_australian_credit	68.2609	1.0748	68.5507	0.8262	68.5507	2.9256	68.6957	1.3939	68.1159	2.8065	68.9855	1.571
statlog_german_credit	77	4.3589	77.4	1.917	76.8	4.0404	77.4	3.3801	77.1	2.2749	77	1.7678
statlog_heart	81.1111	3.5621	81.4815	2.343	80.3704	5.4935	81.4815	5.0715	82.963	3.3127	83.3333	2.6189
tic_tac_toe	88.3017	9.0423	93.101	8.862	87.987	10.7038	91.7479	7.8709	98.1195	1.9779	98.2226	1.9209
titanic	77.3259	16.0188	77.9168	15.5828	77.6901	15.4985	79.0532	15.0381	77.9168	15.5828	78.4623	10.2711
adult	84.282	0.1975	84.6505	0.1594	84.2144	0.2149	84.63	0.1945	84.327	0.279	84.3495	0.2315
connect_4	75.5569	3.7062	75.7464	3.5404	75.4592	3.78	75.7153	4.2827	75.511	3.8167	75.6102	3.7243
hill_valley	81.4318	4.3094	82.1763	4.5884	77.8904	5.3723	81.8485	4.9289	82.345	5.2034	82.9242	5.0465
magic	78.612	15.7624	79.4217	15.3015	78.3596	16.2135	79.4059	15.6682	76.6141	16.3535	76.9664	12.1802
miniboone	82.8393	18.4002	84.1671	17.2489	81.5984	19.1533	83.8526	17.3439	84.4339	16.2213	84.6453	15.5055
mushroom	97.3779	2.5765	99.0151	1.2892	96.3073	3.9179	98.855	1.6016	98.7442	1.7465	98.8672	1.8249
musk_2	84.5909	34.4558	84.5909	24.4228	84.5909	34.4558	85.6212	22.1519	84.5909	34.4558	85.317	26.4714
ozone	97.1217	2.2639	97.1217	2.1594	97.1611	2.2511	97.1611	2.2511	97.1611	2.2511	97.24	2.0916
spambase	88.481	4.7026	89.2203	4.1411	88.1775	5.2705	88.612	5.1656	89.1985	4.1898	89.6106	2.0493
twonorm	51.3514	0.9053	51.4459	1.3519	51.6216	1.1615	51.5811	1.0593	52.1892	0.7946	52.2432	0.584
abalone9-18	95.9035	3.9418	96.0404	3.8631	95.9025	3.5716	96.0404	3.4631	96.1765	3.6227	96.3126	3.3924
aus	86.3768	3.9157	86.9565	2.5102	86.3768	3.5277	86.8116	4.3899	85.6522	2.5824	86.087	2.6736
brwisconsin	90.629	2.6065	90.9221	3.6967	90.4841	6.0049	91.213	4.6945	91.6595	4.8009	91.9483	4.6245
bupa or liver-disorders	73.3333	4.5369	74.2029	3.4601	73.913	2.7113	73.6232	1.6286	74.7826	4.1753	74.7826	4.2992
checkerboard_Data	85.942	4.3053	86.9565	2.7593	86.087	3.2568	86.8116	2.4786	85.5072	2.562	85.6522	2.3756
cleve	81.1469	2.4849	81.8023	1.7427	80.4576	4.2873	82.1469	2.6213	82.8192	2.8433	83.4859	3.9214
crossplane150	62	12.1564	62	12.1564	62	12.1564	62	10.0286	62	12.1564	62	12.1564
ecoli-0-1-4-6_vs_5	98.5714	1.494	98.9286	1.3972	98.9286	1.5972	98.9286	1.5972	98.9286	1.5972	99.2857	1.5972
ecoli-0-1-4-7_vs_2-3-5-6	97.9104	1.335	97.9104	1.335	97.3178	0.6773	97.9104	1.335	97.9192	1.3277	98.5075	1.0554
ecoli-0-1_vs_2-3-5	97.9592	3.5348	98.3673	2.6609	97.9592	3.5348	98.3673	2.6609	98.7755	1.8254	98.7755	1.8254
ecoli-0-1_vs_5	98.75	1.1411	98.75	1.1411	97.9167	2.0833	98.75	1.8634	99.1667	1.1411	98.75	1.1411
ecoli-0-2-3-4_vs_5	98.5122	2.2294	99.5	1.118	98.5	2.2361	99	2.2361	99	2.2361	99.0122	1.3528
ecoli-0-2-6-7_vs_3-5	96.8889	5.7948	97.3333	5.5628	97.3232	4.8166	97.3333	4.6177	98.2222	3.9752	98.2222	3.9752
ecoli-0-3-4-6_vs_5	98.0488	2.0406	98.5366	2.1815	98.0488	2.6718	98.5366	2.1815	98.5366	2.1815	99.0244	1.3359
ecoli-0-3-4-7_vs_5-6	98.8311	1.0672	98.8311	1.0672	98.8311	1.0672	98.8311	1.0672	98.8311	1.0672	98.8311	1.0672
ecoli-0-4-6_vs_5	98.5122	1.3584	98.5244	2.1885	98.5244	1.3473	98.5244	1.1885	99	1.3693	99.0122	1.3528
ecoli-0-6-7_vs_5	98.1818	1.9015	98.1818	1.0164	97.7273	1.6071	98.1818	1.0164	98.1818	1.9015	98.6364	1.2448
ecoli0137vs26	96.4772	3.0561	97.1173	2.6162	96.7998	2.9663	97.1173	2.6162	96.7998	2.9663	97.1173	2.3545
ecoli01vs5	99.5833	0.9317	99.5833	0.9317	100	0	99.5833	0.9317	100	0	100	0
ecoli3	94.3371	4.4091	94.3459	4.0035	94.043	4.2275	94.3459	3.4018	94.3459	3.4018	94.9385	3.0983
ecoli4	99.1089	0.8135	99.1089	0.8135	98.8147	1.2331	99.1089	0.8135	99.1089	0.8135	99.403	0.8175
glass2	92.0487	2.1192	92.0487	2.1192	92.0487	2.1192	92.0487	2.1192	92.0487	2.1192	92.5138	2.0004
haber	74.146	8.0641	74.146	8.0641	74.146	8.0641	74.146	8.0641	74.146	8.0641	74.4685	6.6426
haberman	73.8181	8.0332	74.146	8.0641	74.146	8.0641	74.146	8.0641	74.146	8.0641	74.4685	6.6426
heart-stat	81.4815	3.7037	82.2222	4.4598	80	3.3127	82.963	3.5621	81.8519	3.0429	83.3333	2.268
iono	92.3219	5.9031	93.171	4.7581	94.0201	4.7751	93.7465	6.0777	90.0483	7.9003	92.0322	5.1838
led7digit-0-2-4-5-6-7-8-9_vs_1	96.6216	1.58	96.8488	1.8393	96.6216	1.58	96.6241	2.0952	96.3968	1.8373	96.3968	1.8373
monk1	52.1412	5.306	52.6786	6.0064	52.6786	6.0401	52.5064	3.836	53.2159	6.789	53.2207	5.2456
monk2	68.2204	6.9017	67.5592	6.2258	67.7231	5.2935	67.719	6.5003	68.5551	7.5396	68.8829	6.8224
monk3	52.5225	5.4391	52.1622	3.8802	52.3423	4.9998	52.7027	5.4054	53.2432	6.5926	53.0631	5.1596
new-thyroid1	99.5349	1.04	98.6047	1.2738	99.5349	1.04	98.6047	1.2738	100	0	100	0
pima	71.0916	3.5385	71.089	4.2695	71.2206	2.5043	71.0941	3.5099	71.999	3.1541	72.2647	4.208
ripley	59.84	3.3657	59.84	3.3657	59.84	3.3657	59.84	3.3657	59.84	3.3657	59.84	3.3657
segment0	99.6968	0.1184	99.6968	0.1184	99.6535	0.1934	99.6968	0.1184	99.7401	0.0967	99.7401	0.0967
shuttle-6_vs_2-3	100	0	100	0	100	0	100	0	100	0	100	0
shuttle-c0-vs-c4	100	0	100	0	100	0	100	0	100	0	100	0
sonar	85.5052	8.7141	85.5865	2.9101	83.1243	5.8574	85.0523	6.3716	86.0163	8.012	87.4913	2.0645
votes	97.0115	2.2406	97.0115	1.7682	96.7816	2.7442	97.4713	2.0562	97.0115	3.5983	97.0115	3.5983
vowel	96.4549	2.239	96.5559	2.0115	95.9509	1.132	96.8589	2.1659	96.5569	2.189	97.263	2.2884
wpbc	81.4305	3.8828	81.9568	3.0597	80.4184	4.2533	81.4575	5.5055	78.8664	11.0845	80.9042	8.1087
yeast-0-2-5-6_vs_3-7-8-9	93.7214	2.2892	94.0214	2.0642	93.8204	2.4502	93.6219	2.3102	94.1199	2.2274	94.3199	1.897
yeast-0-2-5-7-9_vs_3-6-8	97.4109	0.8157	97.4114	0.9549	97.4114	1.0767	97.4114	1.0767	97.4119	1.0767	97.5109	0.9288
yeast-0-5-6-7-9_vs_4	93.5544	2.08	93.3711	1.3473	93.9389	1.0797	94.124	1.5831	93.9389	1.2758	93.9407	1.4239
yeast-2_vs_4	96.6933	2.0119	96.6952	2.1241	97.0798	1.5412	97.0817	1.1891	97.0798	1.3798	97.0836	2.1688
yeast1vs7	95.2102	1.6402	95.2102	1.6402	95.4276	1.409	95.2102	1.2284	95.645	1.324	95.8624	1.4118
yeast2vs8	98.1379	1.8496	98.3462	1.5649	98.14	1.8448	98.3462	1.5649	98.5524	1.3856	98.5524	1.3856
yeast3	94.8794	2.0656	95.1488	2.3868	94.8792	2.4891	95.0143	1.967	95.0817	2.1621	95.5531	2.4433

Table 5: Comparison of RVFL, ELM, and BLS with their **`StaR`**-enhanced counterparts on multiclass classification tasks.

Dataset	RVFL		**`StaR`**-RVFL		ELM		**`StaR`**-ELM		BLS		**`StaR`**-BLS	
	Acc.	Std.	Acc.	Std.	Acc.	Std.	Acc.	Std.	Acc.	Std.	Acc.	Std.
abalone	63.7295	1.8436	63.5858	2.724	63.586	1.4052	63.7533	1.5148	63.3458	2.2389	63.6094	2.1706
annealing	89.1899	5.2447	90.4146	5.2285	88.9677	3.9794	90.4146	3.66	90.0807	4.4372	90.1924	4.3932
arrhythmia	70.5812	3.4937	70.7985	3.2655	65.7118	6.1656	68.8181	5.8023	65.0379	2.9768	66.1392	4.1551
balance_scale	98.4	1.2649	97.92	1.2533	98.4	0.8	98.24	1.5388	98.08	1.3387	98.24	0.6693
cardiotocography_10clases	69.1463	4.3501	71.1208	4.2849	70.5569	4.4265	71.2154	4.3552	65.9468	4.6107	66.2289	3.4441
cardiotocography_3clases	85.421	7.4456	86.3153	7.2336	85.7049	8.1929	86.3624	7.9329	85.7514	7.8278	86.0325	7.048
conn_bench_vowel_deterding	95.6566	9.158	95.6566	8.0855	95.6566	7.8046	95.7576	7.1013	95.9596	8.755	96.2626	8.0777
contrac	40.6597	9.9532	41.2708	8.0619	40.7956	10.5615	41.3373	10.4955	44.4707	7.2873	49.0174	9.1506
dermatology	97.2714	1.6665	97.8156	1.5587	96.7308	2.8118	97.8119	2.0793	97.5379	2.2532	98.3562	1.7861
ecoli	61.2072	36.4683	61.5057	22.4895	60.619	36.0715	60.9131	24.4024	60.619	36.0715	61.5101	25.1872
energy_y1	89.0578	5.2589	91.5355	4.4592	89.1868	2.8495	91.1442	2.277	87.8924	5.1619	89.1936	5.0621
energy_y2	90.1002	4.1093	92.7052	3.2735	90.6205	5.5147	91.4057	4.2013	89.9728	2.0933	90.7521	3.9612
flags	54.1296	9.6149	54.1565	5.835	52.0918	8.6148	54.1565	7.7682	52.6316	7.0299	54.6559	8.8818
glass	38.6157	24.7338	38.6268	16.9887	38.1506	26.7812	38.1506	13.7866	40.4873	25.2016	42.3477	20.216
heart_cleveland	60.377	6.0305	60.694	4.6238	58.7268	3.3831	60.3497	5.749	60.3716	4.4715	60.7049	5.579
heart_switzerland	47.2667	13.6756	48.8	5.02	45.6667	11.8697	48.9	9.826	47.3	10.5636	50.4667	9.8759
image_segmentation	87.9654	5.1554	88.8745	4.2107	87.316	5.0707	88.3983	4.4578	88.5281	5.06	88.9177	5.0294
iris	74.6667	20.629	72	17.221	74.6667	17.7326	73.3333	10.1384	77.3333	20.3306	79.3333	15.5278
led_display	73	2.3184	73.4	2.2597	73.3	2.2528	73.4	2.6786	72.5	1.6956	72.6	2.7019
lenses	92	10.9545	96	8.9443	92	10.9545	96	8.9443	92	10.9545	92	7.8885
letter	80.945	1.0325	82.455	1.5357	80.25	1.2946	81.705	1.2236	84.98	0.857	85.18	0.8266
low_res_spect	88.3195	2.5687	89.076	2.2452	88.1361	3.4377	88.7004	1.7656	86.6232	3.1099	86.6355	2.6493
lymphography	87.1264	5.6713	89.1494	4.102	86.4368	6.426	87.8161	5.6725	85.1034	3.1839	85.1264	3.8464
molec_biol_splice	53.605	30.5488	53.7618	21.4272	51.8809	50.1766	53.4796	31.5747	68.6834	7.1531	69.1223	7.7201
nursery	70.4707	4.4066	71.25	4.3915	70.3164	5.1309	72.0062	3.0305	71.088	4.1467	71.5972	5.551
oocytes_merluccius_states_2f	91.9713	3.3966	92.3606	3.9852	91.483	3.2722	92.2645	3.1772	92.1659	3.6618	92.5605	2.4662
oocytes_trisopterus_states_5b	87.8244	4.5992	89.4716	3.1959	86.8384	5.6626	89.4782	5.6082	88.273	4.7203	89.0386	4.2511
optical	97.0996	0.5613	97.153	0.4536	96.3523	0.5731	96.7438	0.5397	96.5658	0.5854	96.726	0.5203
page_blocks	95.432	1.2992	95.2492	1.1708	95.3769	1.6885	95.3404	1.659	95.432	1.2974	95.6877	1.2906
pendigits	98.5626	0.1458	98.8355	0.3747	98.4716	0.5011	98.7172	0.4345	98.9447	0.3109	99.0266	0.2148
pittsburg_bridges_MATERIAL	76.7532	24.3771	75.1948	19.3866	75.8874	26.7058	76.1472	41.333	74.7186	18.6238	76.7532	13.9075
pittsburg_bridges_REL_L	64.1905	14.575	64.1905	11.5735	60.4762	14.2211	65.0476	14.7757	68.0952	8.2065	70.0476	11.0097
pittsburg_bridges_SPAN	60.9942	12.2451	65.3216	5.2697	60.9942	15.5736	65.3801	11.7517	61.9883	9.9908	63.1579	8.3295
pittsburg_bridges_TYPE	42.8571	33.1628	43.8095	25.9513	42.8571	33.1628	42.8571	28.1628	44.7619	8.6504	48.5714	6.2882
post_operative	71.1111	17.3027	71.1111	12.3027	72.2222	18.8398	72.2222	17.1234	70	16.0054	72.2222	12.7135
seeds	89.0476	5.4814	90	4.6844	87.619	5.6844	89.5238	6.2088	90.4762	4.7619	91.4286	2.1296
semeion	88.2609	3.2019	88.072	2.7514	84.6186	3.7976	86.3143	3.2459	87.5704	3.2215	87.8208	3.1315
soybean	89.4461	8.5351	90.3252	8.644	89.0071	9.367	90.775	7.2268	89.2991	8.8551	89.3023	8.0298
statlog_image	95.1082	1.6096	95.9307	1.3724	95.2381	2.0477	95.7143	1.6082	95.9307	1.1289	96.0606	1.1187
statlog_landsat	82.0357	2.5401	81.9891	2.2086	82.2688	2.8535	81.8959	3.1153	82.3155	2.6604	82.5641	3.1507
statlog_shuttle	98.7155	0.0555	98.5948	0.1927	98.7069	0.121	98.6379	0.1467	98.7879	0.138	98.8034	0.1159
statlog_vehicle	81.205	1.8971	84.3954	3.3719	81.913	1.7771	84.749	1.9127	81.6749	3.0966	81.9095	4.1764
synthetic_control	54.5	36.5319	54.6667	25.7052	52.3333	35.2146	55.1667	30.1624	50.5	33.9659	50.5	22.9699
thyroid	95.75	0.6559	96.1389	0.559	95.5556	0.6054	96.0694	0.6223	96.2361	0.5941	96.25	0.7133
vertebral_column_3clases	65.4839	36.3279	65.8065	26.6984	65.4839	36.2024	65.8065	32.3423	69.6774	16.1854	73.871	12.4622
wall_following	78.1537	5.3948	79.1799	4.8636	77.6033	4.3463	78.7401	5.0849	77.9153	6.431	78.282	5.8011
waveform	86.88	0.9418	86.96	0.6986	86.76	0.8649	87.04	0.6269	86.64	0.8444	86.54	0.8306
waveform_noise	86.26	1.2422	86.62	0.676	85.18	1.7754	86.4	0.8031	86.26	1.3221	86.32	1.0592
wine	96.6349	2.3628	97.7619	2.3291	96.0794	2.512	96.6508	2.3196	97.7619	1.2516	97.2063	1.1645
wine_quality_red	59.665	3.604	60.5382	2.9115	59.2884	3.4565	60.4745	3.3594	59.7882	2.4594	60.1656	5.839
wine_quality_white	52.6758	3.4809	53.3905	4.1599	52.574	4.4247	53.1664	4.8736	52.0231	5.464	52.4519	4.6515
yeast	57.01	4.9782	57.6825	3.9308	56.6717	4.1957	57.7505	4.0994	56.807	3.2234	57.6813	3.1397
zoo	94	8.2158	95	7.0711	96	6.5192	95	6.1237	97	6.7082	97	4.4721

Table 6: Comparison of RVFL, ELM, and BLS with their **FLAiR**-enhanced counterparts on binary classification tasks.

Dataset	RVFL		**FLAiR**-RVFL		ELM		**FLAiR**-ELM		BLS		**FLAiR**-BLS	
	Acc.	Std.	Acc.	Std.	Acc.	Std.	Acc.	Std.	Acc.	Std.	Acc.	Std.
acute_inflammation	100	0	100	0	100	0	100	0	100	0	100	0
acute_nephritis	100	0	100	0	100	0	100	0	100	0	100	0
balloons	86.6667	26.6667	100	0	93.3333	13.3333	100	0	93.3333	13.3333	100	0
fertility	90	7.0711	92	6	89	9.6954	92	6	88	9.2736	91	3.7417
parkinsons	84.6154	18.9119	86.1538	16.8998	83.0769	15.856	86.1538	13.626	86.1538	10.9508	90.7692	10.0753
pittsburg_bridges_T_OR_D	92	5.099	94	3.7417	92	5.099	94	3.7417	89	5.831	91	4.899
bank	89.7788	0.3741	90.2212	0.3741	89.7566	0.4566	90.3761	0.2523	89.4469	0.3252	89.8451	0.2362
blood	80.8054	8.3675	81.3423	7.8887	80.6711	8.7958	81.2081	8.1094	77.9866	12.0237	78.7919	9.6383
breast_cancer	70.5263	39.7499	70.5263	39.7499	70.5263	39.7499	76.8421	13.7873	86.3158	16.3601	92.2807	13.7515
breast_cancer_wisc	97.1223	1.6405	97.8417	1.4388	97.2662	1.5363	97.8417	1.365	96.8345	1.7386	97.6978	1.1511
breast_cancer_wisc_diag	97.8761	0.708	98.7611	0.708	97.6991	1.2004	98.7611	0.9025	97.3451	1.371	98.5841	1.2004
breast_cancer_wisc_prog	82.0513	5.8471	84.1026	5.4754	80.5128	7.3604	83.0769	5.2798	79.4872	7.7773	82.5641	4.4114
chess_krvkp	78.6854	6.8081	87.9186	5.0258	76.3693	7.4495	86.1033	5.2554	86.1346	6.0047	91.2676	6.1829
congressional_voting	63.908	2.6809	65.0575	2.2524	63.4483	2.5599	65.0575	2.3668	62.9885	3.2019	64.5977	2.6611
conn_bench_sonar_mines_rocks	64.878	17.8299	73.6585	10.3938	66.8293	8.9416	76.0976	13.3055	84.878	15.0668	92.1951	9.8048
credit_approval	85.5072	11.8185	86.3768	7.4943	85.3623	10.5449	86.9565	7.8315	87.5362	10.0972	87.8261	8.7366
cylinder_bands	67.8431	3.0628	71.1765	2.0188	67.8431	2.4333	71.7647	3.2457	68.2353	6.5796	73.9216	6.25
echocardiogram	86.1538	6.2493	87.6923	6.6172	85.3846	6.1538	86.9231	6.706	86.9231	4.6154	88.4615	6.4358
haberman_survival	76.0656	3.8236	77.377	5.4272	76.3934	4.2243	78.3607	4.4474	76.7213	3.3436	78.0328	2.8583
hepatitis	85.1613	7.2419	87.7419	7.1842	86.4516	7.1842	89.0323	6.6423	85.1613	8.3123	87.7419	10.2822
horse_colic	86.0274	1.8173	87.3973	3.6139	85.4795	3.195	87.3973	2.6563	82.1918	3.5722	85.7534	3.7365
ilpd_indian_liver	73.4483	3.9089	74.4828	3.9917	73.6207	4.2792	74.3103	2.854	71.5517	3.9693	73.2759	3.7378
ionosphere	90.8571	4.2952	92.8571	4.3331	89.1429	6.0339	92.5714	4.899	83.1429	4.0808	87.4286	4.7294
monks_1	74.4144	3.1519	78.018	4.8213	73.6937	5.3268	78.018	5.6578	68.2883	8.2451	76.7568	7.9238
monks_3	87.6364	12.7998	90.1818	11.2581	88.7273	11.0536	91.0909	5.9028	82.3636	2.4121	86.7273	4.2872
oocytes_merluccius_nucleus_4d	83.6275	2.7486	84.5098	0.8547	82.451	2.3894	84.7059	1.4342	80.3922	2.667	84.1176	2.2485
oocytes_trisopterus_nucleus_2f	80.2198	4.7647	82.967	4.7009	79.8901	5.3452	81.6484	3.4854	78.5714	3.2038	79.6703	1.9348
pima	78.6928	2.8218	79.8693	4.2438	78.0392	4.1254	79.7386	2.8936	78.5621	2.3163	79.2157	3.4436
planning	72.2222	4.3033	72.7778	2.0787	72.2222	5.5556	73.8889	1.3608	71.6667	4.4444	74.4444	2.7217
spect	71.6981	5.3367	73.9623	6.0141	71.6981	5.5971	73.9623	8.1286	73.2075	4.8325	76.2264	3.6973
spectf	82.2642	18.9658	81.8868	18.8906	82.2642	18.9658	90.1887	11.283	89.8113	11.7891	92.8302	6.8965
statlog_australian_credit	68.4058	1.9765	69.2754	0.8696	68.5507	1.9765	69.8551	1.344	66.9565	1.344	68.8406	2.1979
statlog_german_credit	76.9	3.2924	78.4	2.1307	77.8	1.5684	78.3	2.4413	77.1	2.6344	77.9	1.9079
statlog_heart	85.5556	3.5909	87.7778	3.6289	85.9259	3.0089	87.4074	3.9545	86.6667	3.5909	88.1481	2.512
tic_tac_toe	98.6387	2.7225	98.8482	2.3037	98.7435	2.5131	98.8482	2.3037	99.3717	1.0152	100	0
titanic	78.3636	13.836	78.9545	13.6148	78.5	13.7763	79.0909	13.5779	78.3636	13.836	79.1364	13.5668
adult	84.7379	0.1617	85.0266	0.176	84.783	0.2682	85.0573	0.2365	86.1699	0.1617	85.2613	0.176
connect_4	75.4408	3.4034	76.7848	4.7466	75.4082	3.4224	76.7123	4.3011	77.0375	3.4034	79.184	4.7466
hill_valley	72.6446	5.1836	75.4545	6.9027	71.9835	4.8289	75.8678	4.5762	73.489	5.1836	76.8032	6.9027
magic	80.2734	13.8329	81.572	12.3175	79.9422	13.7382	81.4616	12.9245	80.964	13.8329	83.7976	12.3175
miniboone	84.7086	14.6623	85.875	13.1032	83.4945	15.9182	85.3206	13.7848	84.8886	14.6623	88.8835	13.1032
mushroom	96.9581	2.9095	99.4089	0.9063	96.4532	2.9981	99.1995	0.9411	97.138	2.9095	101.0654	0.9063
musk_2	84.5792	30.8415	84.5792	30.8415	84.5792	30.8415	84.5792	30.8415	84.6462	30.8415	86.1208	30.8415
ozone	97.1203	2.0253	97.3176	2.0859	97.1203	2.0253	97.3176	1.8737	98.1195	2.0253	97.5392	2.0859
spambase	87.5652	5.1986	89.1739	4.8701	87.8478	5.33	89.3696	5.0002	88.2586	5.1986	89.9997	4.8701
twonorm	97.8784	0.5416	97.9865	0.5512	97.7297	0.4884	97.973	0.5859	98.6952	0.5416	98.6952	0.5512
abalone9-18	96.1644	3.0199	96.8493	2.7602	95.8904	2.9059	96.3014	3.0508	94.7945	4.0079	96.5753	3.0631
aus	87.8261	3.4722	88.6957	2.3188	87.6812	3.6087	88.6957	2.6958	87.2464	2.3188	88.1159	3.3239
brwisconsin	97.3529	1.1005	97.7941	1.2304	97.5	1.282	97.9412	1.265	96.6176	0.5882	98.0882	1.1947
bupa or liver-disorders	75.3623	3.04	77.1014	1.9227	74.7826	2.84	76.5217	2.8102	70.1449	5.6947	72.7536	5.1362
checkerboard_Data	87.971	1.7512	88.5507	2.688	87.6812	2.3814	88.5507	2.688	87.2464	3.0607	88.6957	2.4934
cleve	85.0847	2.7119	87.1186	2.2991	85.0847	2.2486	87.1186	3.3213	86.7797	2.2486	87.7966	1.2684
crossplane150	98.6667	1.633	100	0	99.3333	1.3333	100	0	97.3333	3.8873	100	0
ecoli-0-1-4-6_vs_5	98.5714	2.0825	98.9286	1.4286	98.5714	1.3363	98.9286	1.4286	97.1429	2.1429	98.5714	2.0825
ecoli-0-1-4-7_vs_2-3-5-6	97.6119	0.7312	97.9104	1.5221	97.6119	1.5221	98.209	0.597	95.2239	2.1936	96.7164	0.597
ecoli-0-1_vs_2-3-5	97.9167	1.8634	98.75	1.0206	97.9167	1.3176	99.1667	1.0206	92.0833	1.559	95	2.826
ecoli-0-1_vs_5	98.75	1.6667	99.1667	1.0206	98.75	1.6667	99.1667	1.0206	94.5833	2.826	97.9167	1.3176
ecoli-0-2-3-4_vs_5	98	1.8708	99	2	98	2.9155	99	2	94.5	4.8477	96.5	3.3912
ecoli-0-2-6-7_vs_3-5	98.6364	1.8182	98.6364	1.8182	97.7273	2.4896	98.6364	1.8182	93.1818	4.0656	96.8182	2.7273
ecoli-0-3-4-6_vs_5	98.5366	1.9512	99.0244	1.1949	98.5366	1.1949	99.0244	1.1949	95.122	3.4493	97.0732	2.8444
ecoli-0-3-4-7_vs_5-6	98.4314	0.7843	98.8235	0.9606	98.8235	0.9606	98.8235	0.9606	95.2941	0.9606	96.4706	0.7843
ecoli-0-4-6_vs_5	98	1.8708	99	1.2247	98.5	1.2247	99	1.2247	97.5	1.5811	98.5	1.2247
ecoli-0-6-7_vs_5	98.6364	1.1134	98.6364	1.1134	98.1818	1.7008	98.6364	1.1134	95	4.6355	97.7273	1.4374
ecoli0137vs26	96.7742	2.6989	97.4194	2.1878	97.0968	2.3705	97.7419	1.6448	93.871	2.3705	95.4839	3.1275
ecoli01vs5	100	0	100	0	99.5833	0.8333	100	0	98.3333	1.559	99.1667	1.6667
ecoli3	93.7313	3.4555	94.6269	3.0733	94.3284	3.7044	94.6269	2.9248	89.5522	3.4035	91.9403	2.2338
ecoli4	99.7015	0.597	99.7015	0.597	99.403	0.7312	99.7015	0.597	95.8209	1.9801	97.3134	1.7406
glass2	91.9048	1.1664	93.3333	2.3328	91.9048	1.9048	93.3333	1.7817	91.9048	1.9048	93.3333	2.7766
haber	76.0656	6.9242	78.3607	4.5667	75.7377	6.1688	78.3607	2.1748	77.377	3.9344	78.0328	4.2243
haberman	77.377	7.2131	78.0328	2.4535	76.7213	4.7963	78.3607	4.1988	76.7213	5.0154	77.7049	3.9617
heart-stat	85.5556	2.7217	87.4074	2.1596	86.6667	2.1596	88.1481	2.7716	86.6667	2.1596	88.1481	3.0089
iono	90.2857	6.4776	93.1429	5.2216	89.4286	5.5402	92	5.757	83.1429	4.899	88.2857	6.7249
led7digit-0-2-4-5-6-7-8-9_vs_1	96.8182	1.6701	97.0455	1.5414	97.0455	1.9813	97.2727	1.8464	95.4545	0.7187	96.8182	1.8182
monk1	52.0721	3.7536	53.3333	5.8496	52.7928	4.7875	53.6937	7.0155	52.7928	3.9721	54.0541	5.9487
monk2	87.1667	6.5107	92.8333	3.3993	85	7.9057	92	4.5522	65.6667	4.8132	73.1667	8.0346
monk3	52.7273	4.5997	52.9091	4.9593	52.9091	5.8182	52.7273	3.8996	52.1818	3.1805	53.0909	5.3195
new-thyroid1	99.5349	0.9302	100	0	99.5349	0.9302	100	0	99.5349	0.9302	100	0
pima	78.1699	3.6648	79.4771	1.9651	78.4314	3.6273	79.4771	3.7796	78.5621	3.1859	79.4771	3.1644
ripley	91.44	1.4444	92.08	1.4176	91.36	1.2548	91.84	1.2027	89.44	1.6895	90.72	1.3242
segment0	99.6963	0.1735	99.8698	0.1063	99.7397	0.0868	99.8265	0.0868	97.8308	1.1061	99.6529	0.1735
shuttle-6_vs_2-3	100	0	100	0	100	0	100	0	100	0	100	0
shuttle-c0-vs-c4	100	0	100	0	100	0	100	0	100	0	100	0
sonar	83.4146	7.462	90.7317	2.8444	84.3902	3.9629	90.2439	3.0851	80	4.7294	87.8049	3.4493
votes	97.0115	1.5592	97.7011	2.4111	97.0115	2.0041	97.4713	1.6893	97.2414	1.5592	97.2414	2.6809
vowel	97.1574	2.0954	98.9848	1.0648	97.0558	1.618	98.3756	1.0353	95.6345	2.4576	98.2741	1.5262
wpbc	82.1053	5.8608	83.6842	6.3158	81.5789	6.2275	84.7368	1.9693	79.4737	2.5784	83.1579	4.8809
yeast-0-2-5-6_vs_3-7-8-9	94.3	2.6	94.6	2.4576	94.2	2.1587	94.5	2.5298	93.7	2.874	94.2	2.2045
yeast-0-2-5-7-9_vs_3-6-8	97.3	0.8718	97.5	0.8367	97.1	0.3742	97.5	0.8367	96.6	0.9695	97.3	1.1225
yeast-0-5-6-7-9_vs_4	93.5238	1.1107	94.2857	0.8518	92.9524	0.7619	93.9048	1.2919	92.381	1.4754	93.9048	1.6605
yeast-2_vs_4	96.6667	2.0188	97.451	1.4673	96.4706	1.9212	97.0588	1.3865	92.9412	3.6367	95.6863	0.9998
yeast1vs7	95.6044	0.695	96.2637	0.5383	95.6044	0.9829	95.8242	1.2815	93.8462	1.1207	94.5055	1.39
yeast2vs8	98.125	1.2148	98.3333	1.0623	98.125	1.2148	98.125	1.2148	98.3333	1.0623	98.3333	1.413
yeast3	95.5405	0.7524	95.7432	1.4586	95.4054	2.1853	95.7432	1.1427	94.9324	2.0383	95.9459	1.2087

Table 7: Comparison of RVFL, ELM, and BLS with their **FLAiR**-enhanced counterparts on multi-class classification tasks.

Dataset	RVFL		**FLAiR**-RVFL		ELM		**FLAiR**-ELM		BLS		**FLAiR**-BLS	
	Acc.	Std.	Acc.	Std.	Acc.	Std.	Acc.	Std.	Acc.	Std.	Acc.	Std.
abalone	66.1796	2.1869	66.4192	1.5827	65.8443	1.7095	66.5389	1.6291	64.90957	1.8491	68.40957	3.0414
annealing	88.3799	3.6102	89.162	5.0786	87.2626	7.3726	89.3855	4.714	89.99367	2.1022	93.49367	3.0883
arrhythmia	70	3.3702	71.1111	3.849	66.6667	5.1159	69.5556	4.9988	73.52567	5.4433	77.02567	2.3727
balance_scale	92.8	1.1314	94.72	2.2964	91.52	0.96	94.72	0.8158	83.66787	9.1298	87.16787	9.0989
cardiotocography_10clases	70.3529	4.4644	72.6588	4.5024	69.9765	4.8212	72.7529	4.7139	64.28907	6.0948	67.78907	2.3321
cardiotocography_3clases	87.8118	6.2774	88.5647	5.9201	87.0588	6.2519	88.2353	6.1122	89.93607	5.1923	93.43607	3.715
conn_bench_vowel_deterding	95.4545	7.1923	96.7677	6.4646	95.5556	7.6488	96.6667	6.4171	68.77817	7.8593	72.27817	9.1212
contrac	41.1565	8.7515	42.1769	7.8039	42.381	8.5552	42.585	8.9925	76.08797	17.715	79.58797	15.9253
dermatology	97.8082	0.6711	98.9041	1.0251	97.5342	1.0251	98.6301	0.8664	98.9041	1.0959	100	0.5479
ecoli	62.9851	29.101	64.4776	28.7312	62.9851	29.2385	65.0746	27.8685	56.79267	39.7071	60.29267	15.1329
energy_y1	89.281	4.2679	92.0261	3.5415	89.281	3.1644	91.634	5.2678	89.93087	4.0796	93.43087	3.9346
energy_y2	91.634	2.9346	92.8105	2.952	89.9346	3.7111	92.9412	2.9054	93.85247	5.8372	97.35247	4.684
flags	53.1579	6.5314	57.8947	5.52	53.6842	9.5029	60	6.5314	58.37947	2.8828	61.87947	3.3287
glass	43.3333	10.4762	49.5238	11.5077	41.9048	8.5978	52.8571	18.7718	63.84307	29.9508	67.34307	29.9281
heart_cleveland	61	3.4319	64.6667	5.5176	60.6667	5.2281	62.6667	5.3333	66.74787	3.7417	70.24787	3.4319
heart_switzerland	45	8.0795	50.8333	10.3414	45	8.8976	50.8333	7.1686	50.74787	12.4722	54.24787	10.3414
image_segmentation	88.355	3.9472	90.4762	4.3785	88.355	5.9646	90.3463	4.814	86.65697	3.8487	90.15697	5.1778
iris	94	5.3333	97.3333	3.8873	94.6667	4	97.3333	3.266	75.74787	24.6757	79.24787	13.0979
led_display	73.7	2.7129	74.1	1.7436	73.2	2.5417	74.1	2.1541	79.64787	1.9339	83.14787	1.3565
lenses	95	10	95	10	90	12.2474	100	0	95.74787	12.2474	99.24787	10
letter	82.27	0.9417	85.89	0.9883	81.25	0.9848	84.94	1.2796	69.16287	5.4931	72.66287	5.0006
low_res_spect	89.0566	1.7497	90	3.6096	88.4906	3.1797	90.1887	2.5031	92.54037	4.9202	96.04037	4.6774
lymphography	88.9655	4.0213	90.3448	4.0213	87.5862	3.5166	89.6552	6.1685	94.02377	6.3956	97.52377	5.5097
molec_biol_splice	52.9467	28.2748	56.5517	25.8537	52.3197	15.701	55.7367	25.6339	84.30587	14.1994	87.80587	9.9124
nursery	89.7145	2.3033	90.2855	2.583	89.1049	2.6947	90.6404	1.5282	82.86977	12.338	86.36977	8.8623
oocytes_merluccius_states_2f	92.3529	2.4918	93.0392	2.5827	92.0588	3.2427	93.0392	2.5827	97.41457	2.6307	100	3.3857
oocytes_trisopterus_states_5b	89.011	3.2226	90.7692	2.6783	87.3626	5.5925	89.8901	3.7844	96.18747	3.832	99.68747	4.0634
optical	97.1886	0.7624	98.2918	0.3252	96.4591	0.4918	97.9004	0.3213	96.42407	1.2687	99.92407	2.6173
page_blocks	95.9415	1.0825	96.1426	0.9075	95.8135	1.1597	96.1243	0.9439	99.29447	1.6111	100	2.8105
pendigits	98.6078	0.3531	99.1174	0.1833	98.5987	0.3385	99.1174	0.2006	99.67867	1.4429	100	2.7156
pittsburg_bridges_MATERIAL	84.7619	18.9042	86.6667	16.3299	84.7619	15.1785	87.619	15.2381	74.31927	22.6579	77.81927	14.6844
pittsburg_bridges_REL_L	70	13.0384	75	8.3666	70	16.4317	75	7.746	69.74787	16.2481	73.24787	11.0682
pittsburg_bridges_SPAN	74.4444	5.6656	77.7778	4.969	74.4444	5.6656	76.6667	6.4788	73.52567	8.165	77.02567	6.508
pittsburg_bridges_TYPE	51.4286	19.8406	56.1905	15.4744	49.5238	21.4233	56.1905	17.4054	45.74787	25.8374	49.24787	16.4782
post_operative	71.1111	15.476	73.3333	11.8634	72.2222	14.0546	74.4444	11.4396	75.74787	14.3157	79.24787	9.978
seeds	94.2857	5.5533	95.7143	4.3644	91.9048	3.8686	93.3333	5.0843	90.98597	11.7031	94.48597	8.5041
semeion	89.0566	3.1029	92.327	2.2111	86.1006	0.8054	92.3899	1.8699	92.85477	2.6535	96.35477	3.3986
soybean	90	6.7966	91.4706	4.8239	89.5588	8.0735	92.7941	4.5896	89.71847	8.0198	93.21847	6.4261
statlog_image	94.9784	0.8593	96.5801	0.8372	94.8052	1.4933	96.6667	0.7321	92.06817	2.5033	95.56817	3.3138
statlog_landsat	87.8322	4.084	89.324	3.501	87.2883	3.2769	88.9355	3.7704	88.84037	3.8627	92.34037	4.0807
statlog_shuttle	99.7741	0.024	99.869	0.024	99.7345	0.0383	99.8293	0.0431	94.81167	3.138	98.31167	3.6719
statlog_vehicle	82.4852	2.2329	84.7337	1.7312	82.4852	2.6882	84.3787	2.4137	84.20937	2.2948	87.70937	3.1962
synthetic_control	61.6667	37.5167	62.8333	37.9349	61.3333	37.2178	62.6667	38.2514	53.08117	29.1138	56.58117	18.3267
thyroid	95.0278	0.5935	96.1806	0.7283	94.8472	0.7142	95.9028	0.6086	99.55347	0.78	100	2.3416
vertebral_column_3clases	67.0968	34.3302	67.7419	34.5478	67.0968	34.1021	69.6774	20.4883	70.26397	34.2452	73.76397	21.2217
wall_following	78.7534	5.21	81.8148	4.158	76.7919	3.3207	81.0266	4.4694	74.05217	3.5178	77.55217	3.8862
waveform	86.98	0.7521	87.34	0.6829	86.68	0.9368	87.36	0.731	92.10787	0.8709	95.60787	2.3929
waveform_noise	86.34	0.898	86.72	0.7547	85.3	0.9839	86.46	0.6829	91.60787	0.7283	95.10787	2.3124
wine	96.5714	4.1991	98.2857	3.4286	96.5714	4.5714	98.2857	2.2857	84.03357	8.3983	87.53357	6.6396
wine_quality_red	58.9969	3.6847	60.4389	2.7643	59.5611	3.0002	60.9404	3.0753	64.43127	2.8276	67.93127	3.4968
wine_quality_white	53.7896	3.382	54.5455	3.6367	53.7487	3.7046	54.6476	3.7218	56.00327	3.2871	59.50327	3.756
yeast	58.1081	3.3512	59.4595	3.7438	58.2432	3.6611	59.2568	3.5213	61.82897	2.9297	65.32897	3.5544
zoo	95	4.4721	99	2	96	3.7417	97	4	96	5.831	99.5	5.1912

Table 8: Comparison of dRVFL with its **StaR**- and **FLAiR**-enhanced variants on binary classification tasks.

Dataset	dRVFL		**StaR**-dRVFL		**FLAiR**-dRVFL	
	Acc.	Std.	Acc.	Std.	Acc.	Std.
acute_inflammation	100	0	100	0	100	0
acute_nephritis	100	0	100	0	100	0
balloons	86.6667	26.6667	87.5878	20.7489	100	0
fertility	91	7.3485	91.8245	5.7356	91	7.3485
parkinsons	84.1026	18.5893	85.0808	14.4715	85.1282	16.4902
pittsburg_bridges_T_OR_D	92	5.099	92.8022	3.9874	93	4
bank	90.0664	0.4917	90.9117	0.4068	92.5664	0.512
blood	81.2081	8.1094	82.2508	6.327	83.7081	5.0731
breast_cancer	70.5263	39.7499	71.8071	30.9166	73.0263	24.2378
breast_cancer_wisc	97.4101	1.2544	98.0918	0.9995	99.9101	1.1225
breast_cancer_wisc_diag	98.2301	0.7915	98.8935	0.6398	100	0.8666
breast_cancer_wisc_prog	83.0769	5.5232	84.078	4.3171	85.5769	3.9837
chess_krvkp	89.7966	4.2541	90.6479	3.3308	92.2966	3.5329
congressional_voting	63.2184	2.8155	64.662	2.2127	65.7184	2.2799
conn_bench_sonar_mines_rocks	71.7073	7.1692	72.9617	5.5963	74.2073	5.0374
credit_approval	85.6522	11.3229	86.5959	8.8243	88.1522	7.5413
cylinder_bands	68.0392	5.6353	69.3754	4.4042	70.5392	3.4844
echocardiogram	85.3846	3.7684	86.3343	2.9533	87.8846	3.2014
haberman_survival	75.082	7.0625	76.2612	5.5133	77.582	4.2739
hepatitis	87.7419	5.5499	88.6391	4.3378	90.2419	4.0869
horse_colic	86.5753	2.0133	87.4985	1.5893	89.0753	1.6627
ilpd_indian_liver	72.931	4.9552	74.1582	3.8756	75.431	4.2925
ionosphere	94.2857	3.3806	95.037	2.6519	96.7857	2.8099
monks_1	72.0721	4.5937	73.3184	3.5947	74.5721	3.9139
monks_3	91.0909	7.2134	91.9134	5.6306	93.5909	4.9196
oocytes_merluccius_nucleus_4d	84.5098	1.5686	85.479	1.2437	87.0098	1.2839
oocytes_trisopterus_nucleus_2f	80.1099	3.9986	81.1771	3.1322	82.6099	3.5865
pima	79.085	4.0712	80.175	3.1886	81.585	3.5725
planning	71.6667	6.6667	72.922	5.2057	74.1667	4.9395
spect	72.4528	4.4007	73.6906	3.4447	74.9528	3.9144
spectf	80	18.9658	81.0696	14.7641	82.5	13.0804
statlog_australian_credit	67.8261	1.5609	69.167	1.2377	70.3261	1.3926
statlog_german_credit	77.7	2.1587	78.8209	1.7023	80.2	1.7461
statlog_heart	85.1852	2.6189	86.1393	2.06	87.6852	2.1465
tic_tac_toe	98.7435	2.5131	99.3954	1.9777	100	2.0218
titanic	77.3636	14.4246	78.492	11.2349	79.8636	9.3587

Table 9: Comparison of dRVFL with its **StaR**- and **FLAiR**-enhanced variants on multiclass classification tasks.

Dataset	dRVFL		**StaR**-dRVFL		**FLAiR**-dRVFL	
	Acc.	Std.	Acc.	Std.	Acc.	Std.
abalone	66.0838	0.8715	67.8297	0.9138	69.2838	1.0386
annealing	89.7207	5.2	90.4636	4.2777	92.9207	5.7046
arrhythmia	69.3333	4.1929	71.1201	3.495	72.5333	4.43
balance_scale	93.76	3.1759	95.6589	2.7047	96.96	3.2782
cardiotocography_10clases	74.1176	3.1286	75.1364	2.6679	77.3177	2.9823
cardiotocography_3clases	88.4235	5.8121	89.1235	4.7534	91.6235	5.5402
conn_bench_vowel_deterding	96.9697	6.0606	98.8392	4.9465	100	4.3062
contrac	42.1088	5.7498	44.592	4.705	45.3088	6.2173
dermatology	98.0822	0.6711	98.3904	0.758	100	0.8381
ecoli	63.5821	29.1347	65.4181	22.8788	66.7821	26.1064
energy_y1	91.634	3.7065	92.0905	3.117	94.834	3.4456
energy_y2	91.8954	4.4636	92.3443	3.7054	95.0954	4.9127
flags	53.6842	10.863	55.5153	8.6788	56.8842	10.1346
glass	43.3333	9.4521	43.7787	7.5823	46.5333	7.1218
heart_cleveland	60.6667	5.7349	60.867	4.6934	63.8667	5.4926
heart_switzerland	45.8333	10.5409	47.2362	8.4285	49.0333	7.8567
image_segmentation	91.7749	2.0305	91.8162	1.8145	94.9749	1.9886
iris	93.3333	6.9921	94.3352	5.6704	96.5333	5.8909
led_display	73.2	2.2045	73.7338	1.9498	76.4	2.2092
lenses	95	10	94.6698	8.0081	98.2	7.7568
lymphography	88.9655	4.0213	90.9282	3.3617	92.1655	4.1605
molec_biol_splice	60.721	22.1186	62.0445	17.4261	63.921	16.2151
nursery	89.4522	4.5702	90.3555	3.7882	92.6522	4.466
oocytes_merluccius_states_2f	93.2353	3.6208	92.9351	3.0504	96.4353	3.5861
oocytes_trisopterus_states_5b	88.6813	5.9239	89.1429	4.8403	91.8813	5.9621
pittsburg_bridges_MATERIAL	74.2857	37.0818	75.5595	29.0549	77.4857	34.0734
pittsburg_bridges_REL_L	72	12.083	72.3783	9.6269	75.2	9.0612
pittsburg_bridges_SPAN	71.1111	6.4788	72.6542	5.2716	74.3111	5.4388
pittsburg_bridges_TYPE	42.8571	15.0585	44.2976	11.9393	46.0571	12.9828
post_operative	71.1111	15.476	72.1537	12.2638	74.3111	10.9464
seeds	94.2857	4.1513	94.5794	3.4627	97.4857	4.2917
semeion	95.2201	1.7039	97.3335	1.5607	98.4201	1.9445
soybean	90.7353	6.4873	91.5492	5.2781	93.9353	4.6219
statlog_image	97.5758	0.9224	97.4541	0.9533	100	1.2348
statlog_landsat	90.3341	3.0526	91.784	2.6088	93.5341	3.3573

Table 10: Friedman test results for **StaR**-RVFL vs. RVFL, **StaR**-ELM vs. ELM, **StaR**-BLS vs. BLS, and **StaR**-dRVFL vs. dRVFL on binary and multiclass datasets.

Model	Dataset type	D	χ_F^2	F_F	$F((l-1),(l-1)(D-1))$	Significant difference (As per Friedman test)
StaR-RVFL vs. RVFL	Binary	93	38.7097	65.5971	3.9445	Yes
	Multiclass	53	21.8113	36.3654	4.0266	Yes
StaR-ELM vs. ELM	Binary	93	26.8817	37.4045	3.9445	Yes
	Multiclass	53	27.2453	55.0095	4.0266	Yes
StaR-BLS vs. BLS	Binary	93	40.0108	69.4667	3.9445	Yes
	Multiclass	53	39.92457	158.77632	4.0266	Yes
StaR-dRVFL vs. dRVFL	Binary	36	32.1111	289.0000	4.1213	Yes
	Multiclass	35	24.0286	74.4635	4.13	Yes

Table 11: Friedman test results for **`FLAiR`**-RVFL vs. RVFL, **`FLAiR`**-ELM vs. ELM, **`FLAiR`**-BLS vs. BLS, and **`FLAiR`**-dRVFL vs. dRVFL on binary and multiclass datasets.

Model	**Dataset type**	D	χ_F^2	F_F	$F((l-1),(l-1)(D-1))$	**Significant difference (As per Friedman test)**
`FLAiR`-RVFL vs. RVFL	Binary	93	70.5484	289.0862	3.9445	Yes
	Multiclass	53	51.0189	1.3391e+03	4.0266	Yes
`FLAiR`-ELM vs. ELM	Binary	93	75.8710	407.5028	3.9445	Yes
	Multiclass	53	53	Inf	4.0266	Yes
`FLAiR`-BLS vs. BLS	Binary	93	80.0402	568.1958	3.9445	Yes
	Multiclass	53	53	Inf	4.0266	Yes
`FLAiR`-dRVFL vs. dRVFL	Binary	36	30.2500	184.1304	4.1213	Yes
	Multiclass	35	35	Inf	4.13	Yes

Table 12: Nemenyi post hoc test results for **`StaR`**-RVFL, **`StaR`**-ELM, **`StaR`**-BLS, and **`StaR`**-dRVFL compared to their baseline models on binary and multiclass datasets.

Model	**Dataset Type**	**Average Rank**	**Rank Difference from Baseline**	**Significant Difference (Nemenyi Test)**
`StaR`-RVFL	Binary	1.172	0.650	Yes
	Multiclass	1.160	0.661	Yes
`StaR`-ELM	Binary	1.169	0.600	Yes
	Multiclass	1.167	0.692	Yes
`StaR`-BLS	Binary	1.175	0.652	Yes
	Multiclass	1.186	0.748	Yes
`StaR`-dRVFL	Binary	1.198	0.774	Yes
	Multiclass	1.194	0.720	Yes

To further examine the relative ranking of models, we employ the Nemenyi posthoc test, with results summarized in Tables 12 and 13. This test assesses whether the mean ranks of two models vary beyond a predefined threshold known as the critical difference ($C.D.$). If the deviation between the mean ranks of two models surpasses the $C.D.$, the model with the higher mean rank is considered statistically better than the one with the lower mean rank. The value of $C.D.$ is determined using the formula: $C.D. = q_\alpha\sqrt{\frac{l(l+1)}{6D}}$, where q_α represents the critical value derived from the studentized range statistic divided by $\sqrt{2}$, corresponding to the two-tailed Nemenyi test at a given significance level. At the 5% significance level, the computed critical difference $C.D.$ values for RVFL, ELM, and BLS are 0.2032 for binary datasets and 0.2692 for multi-class datasets. For dRVFL, the corresponding values are 0.3267 and 0.3313, respectively. In all cases, the observed rank differences exceed the critical thresholds, confirming that the performance improvements are statistically significant.

Finally, the win-tie-loss analysis, presented in Tables 14 and 15, further substantiates the consistent superiority of the **`StaR`**- and **`FLAiR`**-enhanced models. According to the win-tie-loss methodology, the null hypothesis assumes equivalence between the two models, implying that each model is expected to win on $D/2$ out of D datasets. At the 5% significance level, a model is considered significantly better if it achieves at least $D/2 + 1.96\sqrt{D}/2$ wins. For RVFL, ELM, and BLS, the

Table 13: Nemenyi post hoc test results for **`FLAiR`**-enhanced RVFL, ELM, BLS, and dRVFL compared to their baseline models on binary and multiclass datasets.

Model	**Dataset type**	**Average rank**	**Rank difference from the baseline**	**Significant difference (As per Nemenyi post hoc test)**
`FLAiR`-RVFL	Binary	1.065	0.871	Yes
	Multiclass	1.009	0.979	Yes
`FLAiR`-ELM	Binary	1.048	0.904	Yes
	Multiclass	1.000	1.000	Yes
`FLAiR`-BLS	Binary	1.036	0.928	Yes
	Multiclass	1.000	1.000	Yes
`FLAiR`-dRVFL	Binary	1.026	0.968	Yes
	Multiclass	1.000	1.000	Yes

Table 14: Win-tie-loss test results comparing **StaR**-enhanced models with their baseline counterparts on binary and multiclass datasets.

Model	Dataset type	Win	Tie	Loss
StaR-RVFL vs. RVFL	Binary	65	23	5
	Multiclass	42	3	8
StaR-ELM vs. ELM	Binary	63	17	13
	Multiclass	44	3	6
StaR-BLS vs. BLS	Binary	68	18	7
	Multiclass	48	3	2
StaR-dRVFL vs. dRVFL	Binary	34	2	0
	Multiclass	32	0	3

Table 15: Win-tie-loss test results comparing **FLAiR**-enhanced models with their baseline counterparts on binary and multiclass datasets.

Model	Dataset type	Win	Tie	Loss
FLAiR-RVFL vs. RVFL	Binary	82	10	1
	Multiclass	52	1	0
FLAiR-ELM vs. ELM	Binary	85	7	1
	Multiclass	53	0	0
FLAiR-BLS vs. BLS	Binary	77	6	0
	Multiclass	53	0	0
FLAiR-dRVFL vs. dRVFL	Binary	33	3	0
	Multiclass	35	0	0

threshold for statistical significance is approximately 55.95 in the binary setting ($D = 93$) and 33.63 in the multiclass setting ($D = 53$). For dRVFL, the corresponding thresholds are 23.88 for binary ($D = 36$) and 23.30 for multiclass classification ($D = 35$). As evident from Tables 14 and 15, both **StaR** and **FLAiR** models consistently surpass their baseline counterparts by a statistically significant margin.

Taken together, these statistical evaluations offer robust empirical support for the effectiveness of the StaR and FLAiR frameworks. The consistent improvements across a wide range of datasets confirm that integrating **StaR** or **FLAiR** into RdNNs leads to significantly enhanced performance, both in terms of accuracy and stability. These results firmly establish the proposed frameworks as principled and effective enhancements for RdNNs.

F CONVERGENCE BEHAVIOR OF **FLAiR**: EMPIRICAL VALIDATION OF MONOTONIC LOSS REDUCTION

To validate the theoretical guarantees of the **FLAiR** framework—particularly Lemma 3, which posits that gradient-based optimization of the input-to-hidden projections consistently reduces prediction error during the warm-up phase, we visualize the evolution of prediction loss over warm-up epochs. Specifically, we aim to empirically demonstrate that **FLAiR** yields a monotonic decrease in loss as the number of warm-up epochs increases. This analysis is conducted using the **FLAiR**-RVFL architecture, which integrates the **FLAiR** mechanism into the standard RVFL model. We evaluate this phenomenon on four datasets—Breast Cancer, Echocardiogram, Statlog Heart, and Titanic—by plotting the prediction loss (measured as the mean squared error between logits and targets) against warm-up epochs ranging from 2 to 10. Experiments are conducted under the same hyperparameter search protocol used for main evaluation, ensuring fair and consistent comparisons. As shown in Figures 1a, 1b, 1c, and 1d, the loss curves for all datasets exhibit a clear and consistent downward trend across increasing warm-up epochs. These observations clearly align with our theoretical formulation: **FLAiR** introduces task-awareness into the random input-to-hidden transformations by optimizing the hidden representations to minimize prediction error. This process enhances the adaptability of RdNNs while preserving their simplicity and computational efficiency. The consistently decreasing loss curves empirically demonstrate that the warm-up phase effectively drives the model toward a more informative and stable feature space.

Figure 1: Warm-up epoch vs. prediction loss for four benchmark datasets under the **`FLAiR`** framework. Consistent loss reduction empirically supports the guarantee stated in Lemma 3.

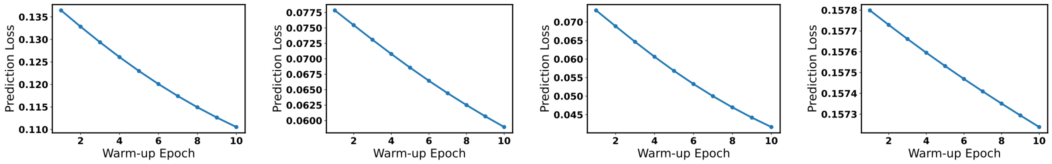

(a) `Breast Cancer` (b) `Echocardiogram` (c) `Statlog Heart` (d) `Titanic`